HHS Public Access

Author manuscript

Nat Neurosci. Author manuscript; available in PMC 2023 August 02.

Published in final edited form as:

Nat Neurosci. 2022 September ; 25(9): 1163–1178. doi:10.1038/s41593-022-01150-1.

Aberrant astrocyte protein secretion contributes to altered neuronal development in multiple models of neurodevelopmental disorders

Alison L.M. Caldwell[1,2], **Laura Sancho**[1,#], **James Deng**[1,2,#], **Alexandra Bosworth**[1,2,#], **Audrey Miglietta**[1], **Jolene K. Diedrich**[3], **Maxim N. Shokhirev**[4], **Nicola J. Allen**[1,*]

[1]Molecular Neurobiology Laboratory, Salk Institute for Biological Studies, 10010 North Torrey Pines Rd, La Jolla, CA, 92037, USA

[2]Neurosciences Graduate Program, University of California San Diego, La Jolla, CA, 92093, USA

[3]Mass Spectrometry Core, Salk Institute for Biological Studies, 10010 North Torrey Pines Rd, La Jolla, CA, 92037, USA

[4]Razavi Newman Integrative Genomics and Bioinformatics Core, Salk Institute for Biological Studies, 10010 North Torrey Pines Rd, La Jolla, CA, 92037, USA

Abstract

Astrocytes negatively impact neuronal development in many models of neurodevelopmental disorders (NDs), however how they do this, and if mechanisms are shared across disorders, is not known. Here, we developed a cell culture system to ask how astrocyte protein secretion and gene expression change in three mouse models of genetic NDs (Rett, Fragile X and Down Syndromes). ND astrocytes increase release of Igfbp2, a secreted inhibitor of IGF. IGF rescues neuronal deficits in many NDs, and we found blocking Igfbp2 partially rescues inhibitory effects of Rett Syndrome astrocytes, suggesting increased astrocyte Igfbp2 contributes to decreased IGF signaling in NDs. We identified increased BMP signaling is upstream of protein secretion changes, including Igfbp2, and blocking BMP signaling in Fragile X and Rett Syndrome astrocytes reverses inhibitory effects on neurite outgrowth. This work provides a resource of astrocyte secreted proteins in health and ND models, and identifies novel targets for intervention in diverse NDs.

Introduction

Despite being caused by diverse genetic mutations, many different neurodevelopmental disorders (NDs) have over-lapping phenotypic neuronal alterations, including stunted axonal and dendritic arbor growth, deficits in synapse formation, and immature dendritic spines[1].

*Corresponding Author: nallen@salk.edu.
#These authors contributed equally

Author Contributions

A.L.M.C. and N.J.A. designed the experiments and wrote the manuscript with input from all other authors. N.J.A. conceived the project. A.L.M.C., N.J.A., J.D., L.S., A.B., A.M., J.K.D. performed experiments. N.J.A., A.L.M.C., J.K.D., J.D. and M.N.S. analyzed data.

Competing Interests

The authors declare no competing interests.

In Rett Syndrome (RTT; Mecp2 loss of function) dendritic arbor complexity and spine density are decreased[2–4]; in Fragile X Syndrome (FXS; Fmr1 loss of function) dendritic outgrowth is stunted and immature spines are increased[5,6]; in Down Syndrome (DS; trisomy chromosome 21) spine density is decreased and immature spines are increased[7]. The phenotypic overlap in these NDs suggests there may be common molecular mechanisms driving alterations. Much ND research has focused on intrinsic changes within neurons, however emerging work has identified alterations to glial cells also play a role[8]. Astrocytes are an abundant class of glial cell and in the healthy brain support neuronal development including through secreted factors. Wild-type (WT) neurons cultured in the absence of astrocytes show reduced survival, stunted neurite outgrowth and defects in synapse formation, whereas the addition of WT astrocytes or astrocyte secreted factors (ACM) is sufficient to overcome these deficits and promote neuronal development[9,10]. Conversely, WT neurons cultured with astrocytes or ACM from FXS, RTT or DS models fail to develop normally, exhibiting stunted neurite outgrowth, decreased synapse formation and immature dendritic spines[8,11–13]. This demonstrates that astrocytes are contributing to aberrant neuronal development in models of NDs through altered release of secreted factors.

This study asks how ND astrocyte protein secretion is altered across multiple models of NDs (FXS, RTT, DS) to identify if there are convergent mechanisms impacting neuronal development[11–13]. We took a proteomics approach as alterations in mRNA do not always correlate with protein changes in neurological disorders, nor to levels of secreted proteins[14,15]. To study astrocytes at a timepoint relevant to neurite outgrowth and synapse formation we developed an immunopanning (IP) procedure to prospectively isolate age and region matched astrocytes and neurons from postnatal day (P)7 mouse cortex, with time and region matching important given astrocytes from different brain regions have significantly different gene expression profiles[16,17]. Using IP to isolate and culture astrocytes has advantages over the classical astrocyte culture method[18,19], including enabling astrocyte isolation at older ages (P7) than the classical procedure where immature progenitors are isolated at P0–1. IP astrocytes are cultured in defined serum-free media which maintains *in vivo* like properties, whereas in the classical procedure astrocytes are cultured in serum which can alter properties, including inducing genes associated with reactive astrocytes which can confound studies of astrocytes in disease settings[18,19].

Using the IP system we generated a resource of protein secretion and gene expression profiles of WT and ND model astrocytes from the developing cortex. We used this resource to identify how astrocytes from FXS, RTT and DS differ in protein secretion from WT, finding unique changes for each disorder, as well as 88 proteins significantly increased in secretion in all 3 NDs. Although gene expression is altered between WT and ND astrocytes, there is little overlap in protein secretion and gene expression changes, highlighting the importance of a proteomics approach when studying secreted proteins. We validated that two of the proteins upregulated in secretion from ND astrocytes, Igfbp2 and BMP6, are upregulated *in vivo* in mouse models of ND, and have negative effects on neuronal development that can be rescued by antagonizing their function. This work has identified how altered astrocyte protein release contributes to aberrant neuronal development in diverse models of NDs, and provides new pathways for therapeutic targeting in these disorders, as well as in sporadic NDs that have shared phenotypic neuronal alterations.

Results

Immunopanned astrocyte and neuron cultures for study of NDs.

To study astrocytes from mouse models of NDs we developed an immunopanning (IP) procedure to isolate astrocytes from the cortex, modifying a protocol for rat astrocytes (see Supplemental Methods)[19,20]. We chose immunopanning as it does not require access to specialized equipment, or the use of transgenic mice expressing fluorescent proteins, so can be widely applied. The cerebral cortices from P7 mice were digested with papain to produce a single cell suspension, which was passed over antibody-coated plates to deplete irrelevant cell types (microglia, endothelial cells, oligodendrocyte precursor cells (OPCs)), with positive selection for astrocytes using an antibody against astrocyte cell surface protein 2 (ACSA2; recognizes Atp1b2) (Figure 1a)[21,22]. IP astrocyte cultures are highly enriched for astrocytes and depleted of other cells, shown by qRT-PCR and immunostaining (Figure 1b,c; Extended Data Figure 1a,b). Astrocytes were cultured for 5–7 days in defined serum-free media with the growth factor HBEGF to promote survival, then switched to protein-free conditioning media for 5 days to collect astrocyte-secreted proteins, referred to as astrocyte conditioned media (ACM). Using protein free media (including carrier-free growth factors) for conditioning is necessary to enable detection of low abundance proteins in complex mixtures using mass spectrometry analysis.

To ask if mouse IP astrocytes are more representative of *in vivo* astrocytes than traditional astrocyte cultures we performed RNA sequencing of astrocytes from 3 conditions: 1) cortical astrocytes isolated at P7 using immunopanning and cultured for 7 days (IP C; as used in this study); 2) astrocytes acutely isolated at P7 using immunopanning (IP A; representative of *in vivo* gene expression); 3) astrocytes isolated and cultured at P1 using the method of McCarthy and de Vellis (MD; method commonly used to culture astrocytes in serum) (Table S1). We calculated differentially expressed genes (DEGs) between IP A and each group, finding MD astrocytes have many more DEGs than IP C (Figure 1d). Genes associated with reactive astrocytes are significantly upregulated in MD astrocytes, and not altered in IP C astrocytes (Figure 1e). These findings are consistent with those from rat astrocytes and demonstrate the validity of using IP isolation and serum-free culturing methods to study astrocyte properties *ex vivo*[19].

We modified the immunopanning protocol to isolate age and region matched neurons from WT P7 mouse cortex, using an antibody against the neuronal protein NCAM-L1 (Figure 1f)[23]. We determined the identity of the neurons by culturing them for 48 hours in the presence of WT ACM (3μg/ml) and immunostaining for MAP2 (label all dendrites) and cortical neuron layer markers (L): Satb2 (L2–5), Ctip2 (L5–6), Tbr1 (L2/3 & 6), Reelin (L1) and GAD (inhibitory interneurons). This showed Satb2 positive cells are most abundant and Reelin positive cells least abundant (Figure 1g; Extended Data Figure 1c), showing IP cortical neuron cultures represent a mix of neurons across layers and classes. To asses neurite outgrowth IP cortical neurons were plated in serum free medium (alone condition) or with WT ACM (3μg/ml), cultured for 48 hours (a timepoint used in previous studies of ND astrocytes), and immunostained for MAP2 (dendrites) and Tau (axons) (Figure 1h,i; Extended Data Figure 1d–f)[24]. We found WT cortical neurons grown in isolation show

minimal neurite outgrowth (total outgrowth = MAP2+Tau), and addition of WT ACM significantly increases this (Figure 1h,i; Extended Data Figure 1d–f), demonstrating that IP WT ACM is supportive of neurite outgrowth.

IP astrocytes reproduce in vivo alterations to ND astrocytes.

WT ACM supports neurite outgrowth, indicating factors secreted by astrocytes are impacting neuronal development. To identify what these proteins are and whether they are altered in ND astrocytes we compared protein secretion and gene expression from astrocytes from 3 mouse models of NDs to strain matched WT control: 1) RTT, Mecp2 KO; 2) FXS, Fmr1 KO; 3) DS, Ts65Dn Down syndrome transgenic with one copy of the duplicated chromosome; 4) WT control, C57Bl6J (Figure 2a; Extended Data Figure 2a). We analyzed astrocytes from Mecp2 and Fmr1 KO mice, as heterozygous cultures would be a mixture of WT and KO cells due to both genes being present on the X chromosome and undergoing random X inactivation, which would mask differences in protein secretion into the media. We used mass spectrometry to identify proteins present in ACM (N=6 cultures/group), detecting 1235 unique proteins in WT ACM at ≥0.01% abundance (Table S2). To determine if protein levels are altered between ACM from WT and each ND we used the T-fold module in Patternlab software, with significance set at $p<0.05$, abundance ≥0.01%, fold change (FC) ≥1.5. To determine gene expression we performed RNA sequencing (N=6 cultures WT, FXS, RTT; 4 DS), detecting 12315 genes in WT astrocytes at FPKM>1 (Table S3). Significance for differential expression between ND and WT was calculated in DESeq2 and defined as $p<0.05$ adjusted for multiple comparisons, expression ≥FPKM 1 and FC ≥1.5.

To ask if overall properties of ND astrocytes are altered we analyzed genes associated with astrocyte function, finding most to be expressed at high levels (Figure 2b,c)[25]. We found no significant differences in marker gene expression (e.g. *Aldh1l1*, *Gfap*), except the calcium binding protein *S100b* which is significantly higher in DS astrocytes, as previously reported[26]. Ion channels and transporters associated with astrocyte function (e.g. *Kcnj10*, *Slc1a2*, *Slc1a3*) are expressed at similar levels, except the glutamate transporter *Slc1a2* (Glt1) which is decreased in FXS, and the GABA transporter *Slc6a11* which is decreased in both FXS and DS. Decreased Glt1 has been reported *in vivo* in FXS mice, however astrocytes cultured from FXS mice using the traditional method do not show this[27,28], demonstrating the benefits of the IP system for maintaining pathological astrocyte properties in culture. Analysis of neurotransmitter receptors showed metabotropic glutamate receptors *Grm3* and *Grm5* (mGluR5) are downregulated in FXS astrocytes, whilst *Grm5* is decreased in DS. As with Glt1, the decrease in mGluR5 has previously been reported in FXS astrocytes *in vivo*[28]. A hypothesis for why ND astrocytes have a negative impact on neuronal development is that they are in a reactive state[29], however we found no difference between WT and ND for a panel of reactive astrocyte genes (Extended Data Figure 2b)[30], suggesting astrocyte reactivity is not involved at this developmental stage.

We determined the most abundant proteins secreted by, and genes expressed by, WT IP astrocytes (Figure 2d,e). Both lists include well known astrocyte-secreted proteins such as *Dbi* (a modulator of GABA receptors), *Apoe* (a component of astrocyte lipid particles) and *Sparc* (negative regulator of synapse formation)[25]. There are only 3 DEGs in the top

15, all in DS astrocytes: an upregulation in *Mt1* and *Mt2* (metallothionein zinc binding proteins) and *Pea15a*. There are more significant differences in protein secretion, including changes shared by all 3 NDs: increases in Igfbp2 (a secreted binding protein for insulin growth factor (IGF)); Cpe (a component of the regulated secretory pathway); and Apoe. We asked if known astrocyte-secreted synapse regulating proteins are present in WT ACM (Figure 2f–j), finding them present at varying abundance: Sparcl1 (silent synapse formation) is most abundant at 0.25%, Gpc4 (immature synapses) is at 0.11%, and Thbs2 (silent synapse formation) is least abundant at 0.002% (Figure 2g)[25], demonstrating that protein abundance is not necessarily indicative of functional effect. Comparing protein levels identified a significant increase in Chrdl1 (synapse maturation) in DS ACM[31], an increase in Gpc4 and Gpc6 in RTT and DS ACM, and an increase in Sparcl1 in RTT ACM. Only *Chrdl1* is also significantly altered at the mRNA level (Figure 2h). Conversely *Thbs2* mRNA is significantly decreased in FXS astrocytes, with no alteration in protein secretion (Thbs2 protein is low so a change may be below threshold). For proteins implicated in developmental synapse elimination a similar pattern is seen, with more differences detected in protein level than gene expression (Figure 2i–j).

Altered protein secretion and gene levels of ND astrocytes.

The above data demonstrate that IP astrocytes maintain many features of *in vivo* astrocytes, further validating them as a system to identify altered astrocyte protein secretion and gene expression in models of NDs. Therefore we asked how astrocytes from each individual ND are altered from WT by determining significantly upregulated and downregulated secreted proteins and genes, as well as the overlap between all NDs and WT for each category (Tables S5, S6, S7, S8, S9).

In FXS we found 131 proteins and 547 genes increased compared to WT, with only 4 factors (3.1%) upregulated at both protein and mRNA levels, including *Bmp6* (regulates astrocyte maturation) and *Sema3e* (secreted semaphorin that inhibits neurite outgrowth) (Figure 3a,b; Extended Data Figure 3a,b)[32,33]. 108 proteins and 246 genes are decreased in FXS, with only 4 targets (3.7%) overlapping (Figure 3a,b; Extended Data Figure 3a,b). We found a significant decrease in *Fmr1* mRNA in FXS astrocytes, as would be predicted. Ntf3 (neurotrophin 3) has been reported to be increased in secretion from FXS astrocytes and to inhibit neurite outgrowth, however we could not detect Ntf3 protein in ACM[34]. *Ntf3* mRNA is present in astrocytes at low levels, with a trend towards an increase in FXS. Panther Pathway analysis of proteins increased in FXS ACM identified the Alzheimer disease-amyloid secretase pathway, blood coagulation pathway, and regulation of IGF transport/uptake by Igfbp (Figure 3k).

In RTT 187 proteins and 49 genes are increased, with no overlap between the mRNA and protein changes (Figure 3c,d; Extended Data Figure 3c,d). Conversely, 200 proteins and 29 genes (including *Mecp2*) are decreased in RTT, with an overlap of 1 target (*Ktcd12*) (Figure 3c,d; Extended Data Figure 3c,d). Pathway analysis of proteins increased in RTT ACM identified the Alzheimer disease-amyloid secretase pathway, integrin signaling pathway, and regulation of IGF transport/uptake by Igfbp (Figure 3k).

In DS there are 272 proteins and 408 genes increased compared to WT, with an overlap of 34 targets (12.5%) (Figure 3e,f; Extended Data Figure 3e,f). As with FXS, the overlap includes *Sema3e* and *Bmp6*. 500 proteins and 249 genes show a decrease in DS ACM, with 11 targets (2.2%) overlapping (Figure 3e,f; Extended Data Figure 3e,f). We asked if the 150 genes that are triplicated in the Ts65Dn mouse model are upregulated in DS astrocytes, finding 97 of the genes are expressed by DS astrocytes at FPKM >1, with 51 genes (53%) significantly upregulated (Table S4). Conversely, only 9.8% of the genes and 1.5% of the proteins upregulated are represented by triplicated genes, showing a broader dysregulation is occurring. Several genes known to be associated with DS have increased mRNA, including *App* and *Adamts1*[35], and App is also increased at the protein secretion level. Increased levels of Mt3 and Efemp1 proteins have been reported in astrocytes in DS patients, and we detected increased levels of both in DS ACM[35,36]. Pathway analysis of proteins increased in DS ACM identified the amyloid secretase pathway in Alzheimer's disease, integrin signaling pathway, and regulation of IGF transport/uptake by Igfbp (Figure 3k).

We next asked whether there are proteins or genes that show common changes in all NDs, finding 88 proteins and 11 genes increased in all 3 NDs vs. WT, with no overlap in protein and mRNA changes (Figure 3g–j;Table S9). In contrast, only 32 proteins and 1 gene show a decrease in all 3 NDs compared to WT, with no overlap in protein and mRNA (Extended Data Figure 3g–j). Analysis of sub-cellular localization of the up and down-regulated proteins by Uniprot determined 95% of upregulated proteins are found outside the cell (dense core vesicle, lysosome, exosome, plasma membrane) whereas only 41% of downregulated proteins are annotated as extracellular (Table S5). Pathway analysis of upregulated proteins identified the Alzheimer disease-amyloid secretase pathway, regulation of IGF transport and uptake by Igfbps, and regulation of the complement cascade, whereas downregulated protein pathways were linked to ion homeostasis and hedgehog signaling (Figure 3k; Extended Data Figure 3k; Table S6). Pathway analysis of the gene expression changes found a decrease in both cadherin signaling and Wnt signaling in FXS and RTT astrocytes (Extended Data Figure 3k; Table S8).

Excess Igfbp2 in ACM inhibits neurite outgrowth.

The mutations present in RTT, FXS, and DS are associated with increased expression of genes and/or proteins. Mecp2 (RTT) is a transcriptional repressor, Fmr1 (FXS) is a translational repressor, and in DS there is triplication of genes[2,5,7]. We therefore focused on proteins upregulated in all three NDs for functional testing, selecting candidates based on potential to regulate neurite outgrowth and synapses. We asked if Igfbp2 (insulin like growth factor binding protein 2) acts on neurons to inhibit neurite outgrowth due to its role as an inhibitor of IGF[37]. We asked if Cpe (carboxypeptidase E) inhibits neurite outgrowth, as neurons in adult mice lacking Cpe show more complex dendritic arbors[38]. As BMP signaling induces astrocyte structural maturation[33], we asked if BMP6 is acting on astrocytes and upstream of altered astrocyte protein secretion that negatively impacts neural development.

We first asked if increasing protein levels of candidate neurite inhibitory factors Igfbp2 or Cpe in WT ACM is sufficient to inhibit WT neurite outgrowth. Treating neurons with Igfbp2

in the absence of ACM had no effect on neurite outgrowth, whereas adding Igfbp2 to WT ACM blocked the neurite-outgrowth promoting effect (Extended Data Figure 4b,c). Adding Cpe to WT ACM had no effect on the ability of WT ACM to support neurite outgrowth, although CPE by itself did promote neurite outgrowth (Extended Data Figure 4b,c). This identifies increased levels of Igfbp2 but not Cpe in ACM as a potential mediator of inhibited neurite outgrowth in NDs. We found Igfbp2 is a highly abundant protein in WT ACM that is further upregulated in all 3 NDs (% of total ACM: WT 2.67%, FXS 4.60%, RTT 4.99%, DS 6.16%; Figure 4b,c). Igfbp2 binds IGF1&2 in the extracellular space, inhibiting their action by preventing interaction with the IGF receptor (Figure 4a)[37]. Activation of the IGF pathway in neurons has positive effects, including promoting cellular survival and neurite outgrowth (Figure 4a)[37], and treatment with IGF1 can decrease neuronal deficits in both RTT and FXS[37], leading us to hypothesize that increased release of Igfbp2 from ND astrocytes is inhibiting IGF signaling in neurons and contributing to stunted neuronal development. To address this we treated WT neurons with WT ACM+Igfbp2+IGF1, finding the addition of IGF1 was sufficient to decrease the inhibitory effect of excess Igfbp2 in WT ACM, suggesting Igfbp2 is inhibiting neuronal outgrowth by preventing IGF1 from signaling to neurons (Extended Data Figure 4b,c). To investigate this further we used an anti-Igfbp2 neutralizing antibody (Igfbp2-Ab) that prevents Igfbp2 from binding to IGF. WT ACM+Igfbp2+Igfbp2-Ab no longer inhibited neurite outgrowth, providing further evidence that the inhibitory effect of Igfbp2 is through its actions on IGF signaling (Figure 4d,e; Extended Data Figure 4e,f). A control non-targeting antibody had no effect on WT neurite outgrowth (Extended Data Figure 4g).

Given these *in vitro* findings we next determined if Igfbp2 is expressed by astrocytes in the developing cortex at P7, the age when astrocytes are isolated for experiments. We performed single molecule fluorescent in situ hybridization (smFISH) for *Igfbp2* mRNA in the P7 visual cortex of Aldh1l1-GFP mice to label astrocytes, along with probes for neurons (*Tubb3*) and OPCs (*Cspg4*). This showed astrocytes in all cortical layers express *Igfbp2* mRNA (Figure 4f). Quantification of *Igfbp2* mRNA in L2/3 showed an enrichment of *Igfbp2* in astrocytes compared to other cell types (Figure 4f,g; Extended Data Figure 4d), validating published RNA sequencing data showing astrocytes are a major source of Igfbp2 in the developing cortex (Extended Data Figure 4a)[39].

We asked if Igfbp2 protein is increased in the extracellular space *in vivo* in mouse models of NDs, which would suggest an increase in secretion occurs *in vivo* as well as *in vitro*. Each ND model was crossed to Aldh1l1-GFP mice to visualize astrocytes, and immunostaining for Igfbp2 performed at P7 (matching the age of isolation for culture) and visualized using confocal imaging of L2/3 of visual cortex. We first analyzed RTT mice due to the strong links between aberrant IGF signaling and RTT[37], and compared male littermate Mecp2+/y;Aldh1l1-GFP (WT) and Mecp2-/y;Aldh1l1-GFP (KO; RTT). We separately analyzed Igfbp2 present within (intracellular, colocalized with GFP) and surrounding (extracellular, no overlap with GFP) astrocytes. This revealed an increase in Igfbp2 levels in the extracellular space, with no significant change in the volume of Igfbp2 within astrocytes (Figure 4h–j). In addition, the extracellular Igfbp2 protein has a more punctate distribution in the Mecp2 KO than WT, where immunostaining is diffuse. To ask if this also occurs in the other ND mouse models we performed the same analysis comparing

littermate WT and Fmr1 KO (FXS) or transgenic Ts65Dn (DS) mice. In FXS there is no significant increase in either extracellular or intracellular Igfbp2 (Figure 4h–j). In DS there is large variability in the level of e.c. Igfbp2 across replicates compared to other NDs, and a significant increase in intracellular Igfbp2 (Figure 4h–j). This demonstrates that Igfbp2 is increased *in vivo* in both RTT and DS, though in different compartments.

Blocking Igfbp2 in RTT reduces neural developmental deficits.

To determine if increased levels of Igfbp2 in ND ACM are contributing to the impact of ND ACM on neurite outgrowth we asked if adding the Igfbp2 blocking Ab would rescue the outgrowth deficit induced in WT neurons. WT neurons cultured with RTT ACM did not show a significant increase in neurite outgrowth compared to neurons alone, whereas the addition of the Igfbp2-Ab to RTT ACM induced a significant increase in neurite outgrowth that partially rescued the deficit (Figure 5a,b; Extended Data Figure 5a,b). WT neurons cultured with FXS ACM did not show a significant increase in neurite outgrowth compared to neurons alone, demonstrating that FXS ACM is not supportive of neurite outgrowth, however addition of the Igfbp2-Ab to FXS ACM did not significantly enhance neurite outgrowth (Figure 5c,d; Extended Data Figure 5c,d). We found that DS ACM supports WT neurite outgrowth to a comparable level as WT ACM, and that addition of the Igfbp2-Ab to DS ACM has no effect on neurite outgrowth (Figure 5e,f; Extended Data Figure 5e,f). These results show that the effect of ND ACM on WT neurite outgrowth is variable, being most severe for RTT ACM, less severe for FXS ACM, and no effect detected with DS ACM (the reported phenotype in DS is a mild 15% decrease[40]). Of note there is a significant increase in IGF1 secretion from DS astrocytes (Figure 4b), which may compensate for the increased Igfbp2 level.

To determine if Igfbp2 is inhibiting neuronal development *in vivo* in RTT we asked if delivering the Igfbp2-Ab to RTT mice would rescue reported *in vivo* phenotypes. We focused on decreased neuronal cell body size as this has been shown consistently both *in vitro* and *in vivo*, in human neurons and multiple RTT mouse models[4,24,41]. We first asked if the Igfbp2-Ab could rescue decreased neuronal cell body size *in vitro* by analyzing cell body size in the dataset presented in Figure 5a,b. This showed WT neurons cultured with RTT ACM have smaller cell bodies than those cultured with WT ACM, and that this decrease is reduced by adding the Igfbp2-Ab to RTT ACM (Figure 5g; Extended Data Figure 5g). This is consistent with studies showing deficits in neuronal cell body size in RTT *in vitro* can be rescued with Igf1 treatment[24,41]. We then asked if we could detect a decreased cell body size at P7 in cortical neurons *in vivo* in RTT mice, which has previously been reported in layer 5 neurons at P30 and P60 in this specific mouse model[4]. Neurons in the visual cortex of littermate WT (Mecp2+/y) and RTT (Mecp2-/y) mice were labeled by local injection of AAV-synapsin-GFP at P2, and analyzed at P7 (Figure 5h). We separately analyzed the area of individual neuronal cell bodies in upper (L2/3) and deep (L5) cortical layers, and found a significant decrease in cell body size in deep layer neurons (Figure 5i,j) but not upper layer neurons (Extended Data Figure 5i,j) in RTT mice. We next asked if the Igfbp2-Ab would impact on cell body size by injecting either the Igfbp2-Ab or the isotype control antibody into littermate RTT mice (Mecp2-/y), along with AAV-synapsin-GFP to label neurons (Extended Data Figure 5h). This showed that RTT mice injected with the

Igfbp2-Ab had larger neuronal cell bodies in deep cortical layers than those injected with the control antibody (Figure 5k,l), with no difference detected in upper layer neurons (Extended Data Figure 5k,l). Together this shows that blocking the actions of Igfbp2 *in vitro* and *in vivo* during early development is beneficial for neuronal growth in RTT.

Activating WT astrocyte BMP signaling mimics ND astrocytes.

Given the partial rescue of WT neurite outgrowth by blocking Igfbp2 in RTT ACM, and the lack of effect of blocking Igfbp2 in FXS ACM, this led us to hypothesize that combined altered release of multiple proteins from ND astrocytes is responsible for fully impacting neurite outgrowth. We identified that BMP6 protein is increased in ACM from all 3 NDs vs WT (Figure 6b). BMP signaling is sufficient to induce morphological maturation of astrocytes, so we focused on BMP signaling in ND astrocytes themselves[33]. We detected a significant increase in expression of BMP target genes *Id3*, *Id4*, and *Smad9* in astrocytes from FXS and DS, with a trend towards increased *Id3* and *Smad9* in RTT astrocytes (Figure 6c). As canonical BMP signaling regulates expression of many genes, we hypothesized that enhanced BMP signaling in ND astrocytes may be upstream of protein secretion changes in these disorders.

Astrocytes *in vivo* express components of the canonical BMP pathway (Extended Data Figure 6a). To determine if the BMP pathway is upregulated in ND astrocytes *in vivo,* we examined expression of phosphorylated SMAD 1/5 (pSMAD) in astrocytes in the visual cortex of Fmr1 KO and WT littermates at P7 (FXS). pSMAD is a downstream target of BMPs, and an increase in canonical BMP signaling is reflected by increased pSMAD translocation to the nucleus (Figure 6a)[42]. We compared male littermate Fmr1+/y;Aldh1l1-GFP (WT) and Fmr1-/y;Aldh1l1-GFP (KO) mice at P7 by immunostaining for pSMAD in sections of visual cortex, visualized with confocal imaging. We analyzed the total number of astrocytes and the number of astrocytes positive for pSMAD, identifying a significant increase in the fraction of astrocytes positive for pSMAD in the cortex in FXS (Figure 6d,e). These results demonstrate increased BMP signaling is occurring *in vivo* in astrocytes in FXS KO mice at P7, supporting the hypothesis that aberrant BMP signaling is involved in this disorder.

To ask if increased BMP signaling is upstream of protein secretion changes that negatively impact neuronal development we treated WT astrocytes with BMP6 during the conditioning period, and compared them to astrocytes from the same culture left untreated (Figure 6f). WT astrocytes treated with BMP6 showed distinct changes in morphology (thinner elongated processes), and expressed higher levels of Aqp4 and GFAP protein compared to untreated astrocytes (Extended Data Figure 6b,c), reproducing the finding that BMP signaling induces structural maturation of astrocytes[33]. We used mass spectrometry and RNA sequencing to ask if protein secretion and gene expression of WT astrocytes is altered by treatment with BMP6 (N=6 cultures; Figure 6f; Tables S2, S3). BMP6-treated astrocytes show increased expression of genes associated with astrocyte maturation including *Aqp4*, *Apoe* and *Aldoc*. Genes downregulated include *Grm3* and *Grm5*, a change similar to that seen in FXS astrocytes (Figure 6g). BMP6 treatment did not alter the majority of synaptogenic factors produced by astrocytes, except for a significant increase in protein

secretion and gene expression of *Sparcl1* (Figure 6h,i). BMP6-treated astrocytes secrete significantly more complement component proteins associated with synapse elimination, including C1sa, C3, and C4b, with a corresponding increase in gene expression for *C1sa* and *C3* (Figure 6j,k). Overall, BMP6 treatment induced a significant increase in secretion of 129 proteins and expression of 773 genes, with 45 (34.9%) factors overlapping (Table S5,7,9) (Figure 6l,m). We found a significant decrease in secretion of 273 proteins and a decrease in 731 genes, with 18 (6.6%) factors overlapping (Extended Data Figure 6d,e).

Blocking ND astrocyte BMP signaling reduces neural deficits.

Given our hypothesis that increased BMP signaling is upstream to alterations in ND astrocytes, we compared the proteins altered in secretion in all 3 NDs with those altered by BMP6 treatment of WT astrocytes. 38 of the 88 proteins that are increased in ND ACM are also increased in BMP6-ACM (43.2%), whereas 14 of the 32 downregulated proteins are also downregulated by BMP6 (43.8%) (Figure 7a; Extended Data Figure 7a; Table S5). Of the 11 genes that show increased expression in all NDs compared to WT, 4 of them are also increased in BMP6-treated astrocytes, and the 1 gene showing decreased expression in all NDs is decreased following BMP6 treatment (Figure 7b; Extended Data Figure 7b). This shows a strong overlap in the protein secretion and gene expression profiles of ND astrocytes and WT astrocytes treated with BMP6, indicating that BMP signaling may be upstream of some protein alterations in NDs. Interestingly Igfbp2 and Igfbp5 both show increased secretion from BMP6-treated WT astrocytes, matching the change seen in NDs (Figure 7c). Pathway analysis of genes upregulated by BMP6 treatment also identified the Igfbp pathway (Table S8), providing further support for BMP6 inducing upstream changes in astrocyte function that contribute to aberrant IGF signaling in NDs.

Due to the overlap in altered protein secretion induced in WT astrocytes by BMP6-treatment with those seen in ND ACM, we asked if ACM from BMP6-treated WT astrocytes is supportive of WT cortical neuron outgrowth. Neurons were cultured for 48 hours alone, with WT ACM or BMP6-ACM, demonstrating that BMP6-ACM is not able to enhance neurite outgrowth whereas WT ACM can (Figure 7d,e; Extended Data Figure 7c,d). As we had identified that Igfbp2 is downstream of BMP signaling, and that blocking Igfbp2 with a neutralizing antibody is sufficient to overcome its inhibitory effects, we next asked if adding the Igfbp2-Ab to BMP6-ACM would rescue the inhibition. This showed that the Igfbp2-Ab is sufficient to diminish the inhibitory effect of BMP6-ACM on neurite outgrowth (Figure 7f; Extended Data Figure 7e).

We next asked if inhibiting BMP signaling in ND astrocytes would rescue the negative effects of ND ACM on WT neurite outgrowth. We first focused on FXS as we identified increased BMP pathway activation in astrocytes both *in vitro* and *in vivo* (Figure 6b–e). We isolated FXS astrocytes and treated half of them during the conditioning period with the secreted BMP inhibitor noggin to bind BMPs and prevent BMP-receptor interaction, while leaving the other half untreated (Figure 7g)[42]. ACM from untreated FXS astrocytes did not induce a significant increase in WT neurite outgrowth compared to neurons alone, whereas ACM from FXS astrocytes treated with noggin supported neurite outgrowth to a level indistinguishable from WT ACM (Figure 7h,i; Extended Data Figure 7f,g). To ask if noggin

is having a direct effect on neurons independent of astrocytes we added purified recombinant noggin directly to neurons at the time of ACM treatment. This did not enhance neurite outgrowth, indicating that it is the effects of noggin on FXS astrocytes during conditioning that allows noggin-treated FXS ACM to support neurite outgrowth (Extended Data Figure 7i,j). As the Igfbp2-Ab overcomes some of the inhibitory effect of both RTT ACM (Figure 5a,b) and BMP6-ACM (Figure 7f), we asked if treating RTT astrocytes with noggin during the conditioning period would also be beneficial to neurite outgrowth. This showed that as with FXS, inhibiting BMP signaling in RTT astrocytes is able to diminish the inhibitory effect of ACM on neurite outgrowth (Figure 7j; Extended Data Figure 7h). These results support a critical role for increased BMP signaling in astrocytes in ND in regulating aberrant protein secretion, including Igfbp2, that leads to inhibition of neuronal development.

Discussion

This work has generated a resource to ask how alterations to astrocyte protein secretion contribute to aberrant neuronal development in diverse models of NDs. We developed an approach to isolate cortical astrocytes and neurons from mice at the end of the first postnatal week, a time point when astrocytes regulate neuronal outgrowth and synapse formation *in vivo*. We maintained the astrocytes in culture in defined conditions that maintain their *in vivo* properties and prevent them from becoming reactive. By combining quantitative mass spectrometry analysis of proteins secreted by astrocytes with RNA sequencing analysis of gene expression, we identified the normal protein secretion and gene expression profile of astrocytes at this timepoint, along with how these are altered in multiple models of genetic NDs. We identified a number of differences in both protein secretion and gene expression between each individual ND and WT, as well as 88 proteins upregulated in secretion from all 3 NDs. Further testing showed two of these upregulated proteins, Igfbp2 and BMP6, have negative effects on neuronal development.

While we identified many alterations in protein release from ND astrocytes, the majority of these changes do not show a corresponding alteration in gene expression. This disconnect between proteomic and gene expression alterations in neurological disorders has also been observed in whole tissue, for example in Alzheimer's disease[15]. This highlights the importance of a proteomics approach when studying inter-cellular signaling interactions, particularly for astrocytes, a cell type specialized for secretion[14,43]. Applying new technologies such as proximity biotinylation (BioID) to label cell-type specific secreted proteins *in vivo* will enable investigation of the extent of protein secretion alterations occurring in neurological disorders in intact tissue[44]. Proteins increased in release from ND astrocytes come from multiple sources including dense core vesicles, lysosomes, exosomes and cleaved membrane proteins, indicating an overall change to cell state occurs. Possible mediators of this state change include upregulated BMP signaling (studied here), and another candidate is downregulated Wnt signaling, detected in astrocytes in all NDs.

Increased BMP pathway activation is likely upstream of approximately half the altered protein release from ND astrocytes, including Igfbp2, shown by the overlap in protein profiles of ND astrocytes and BMP-treated astrocytes. Further, treating ND astrocytes with the secreted BMP antagonist noggin, which we chose for its potent BMP neutralizing

activity, reduced the negative effect of ND astrocytes on WT neuron development. It is likely *in vivo* in the developing cortex other BMP antagonists regulate BMP signaling, for example the secreted BMP antagonist Chrdl1 is enriched in astrocytes in upper layers of cortex[31,45]. Bmpr2 is a target of Fmr1, and there is a partial rescue of spine deficits in FXS mice that are heterozygous for Bmpr2, due to non-canonical BMP signaling[46]. Our data suggest a role for canonical BMP signaling in astrocytes should also be considered as mediating altered development in NDs.

IGF signaling is altered in multiple NDs, however there is not a consistent alteration in IGF1 itself[47], suggesting other factors contribute to the signaling deficit. In RTT models we found increased astrocyte-derived Igfbp2 is contributing to stunted neural development by acting as an inhibitor of IGF, suggesting increased levels of Igfbps contribute to deficient IGF signaling in NDs. In Pallister-Killina syndrome, a disorder with impaired growth and intellectual impairment, Igfbp2 is increased in serum of some patients[48], and in RTT mouse models and patients Igfbp3 is increased in the brain[49]. We identified the Igfbp-IGF pathway as altered in all NDs, but to varying degrees, with the most alterations in RTT and least in DS. Importantly we found the Igfbp2 blocking antibody only increased the size of neurons that were smaller in RTT compared to WT (deep layers), and had no impact on cells that were the same size (upper layers) prior to manipulation, suggesting this approach does not cause inappropriate cell growth. Future work should address whether the differential impact of RTT on neuronal size across layers is maintained across development, and what underlies it, for example are there differences in basal IGF signaling in neurons in different layers? Our findings suggest development of compounds to block the interaction of specific Igfbps with IGF to liberate IGF in the appropriate location for it to signal may provide a new approach to enhance IGF signaling in multiple NDs.

In addition to Igfbp2 and BMP6 there are other proteins altered in ACM from all 3 NDs that may contribute to aberrant neuronal development. These include upregulation of class 3 secreted semaphorins, known inhibitors of neurite outgrowth[32]; neuronal Sema3f is linked to both RTT and FXS[50,51]. Downregulated proteins of interest include Sulf2, Hdgfrp3, and Ptn, all of which support neuronal development and neurite outgrowth[52–54], so their deficiency may contribute to the failure of WT neurons to develop in the presence of ND ACM. Future analysis will assess neuronal spines and synapses to determine how alterations to astrocytes in NDs impact later stages of development. It is also important to determine how WT astrocytes are able to overcome the intrinsic reduction in growth seen in neurons that carry ND mutations i.e. what are the pro-growth factors these astrocytes are releasing? In addition, it is important to ask whether the factors we identified in ND astrocytes impact ND neurons themselves. Our experiments in RTT mice *in vivo* address this question for Igfbp2 by demonstrating the Igfbp2 blocking antibody can overcome deficits in neuronal cell body size in neurons deficient in Mecp2. Furthermore, astrocytes are not always inhibitory to neurons in NDs. In Costello Syndrome, astrocytes increase neurite outgrowth and synapse formation and upregulate different proteins including agrin, brevican and neurocan[55]. This exemplifies the importance of using a shared phenotype for comparative studies of astrocytes across NDs to identify changes that are likely to impact the same pathways in neurons.

We found an upregulation of the Alzheimer's disease-amyloid secretase pathway, including increased secretion of App, Apoe and Clu, from astrocytes in all 3 NDs. App is known to be increased in DS as it is present on the triplicated chromosome[35], and is also a target of Fmr1 and increased in Fmr1 KO neurons[56]. Beyond development, DS is associated with early onset Alzheimer's Disease, whereas fragile X associated tremor ataxia syndrome (FXTAS) can occur in people with Fmr1 mutations[57]. In addition, Igfbp2 is increased in the cerebrospinal fluid of patients with Alzheimer's disease[58]. This demonstrates upregulation of proteins associated with neurodegeneration is also occurring in neurodevelopmental disorders, and suggests these proteins may represent a general dysregulation of astrocytes in neurological disorders that occur across the lifespan.

The combination of a physiologically relevant cell culture system with quantitative proteomics of secreted proteins has enabled identification of how astrocytes alter their interaction with neurons in multiple models of genetic neurodevelopmental disorders. This has identified candidate non-neuronal proteins and pathways that can be targeted in these disorders, as well as in disorders of unknown cause with shared phenotypes, in order to correct aberrant neuronal development and function.

Methods

Step by step protocols for immunopanning isolation of mouse astrocytes and neurons are available as Supplementary Methods. Other reagent requests should be sent to nallen@salk.edu.

Animals

All animal work was approved by the Institutional Animal Care and Use Committee (IACUC) of the Salk Institute for Biological Studies.

Mice

Mice were housed in the Salk Institute animal facility at a light cycle of 12 hr light: 12 hr dark, temperature range of 69–71F and humidity range of 47–60%, with access to water and food ad libitum.

Wild-type (WT) mice—WT C57BL/6J (Jax 000664) mice were used to isolate WT astrocytes and neurons. Both male and female mice were used for astrocyte and neuron isolation.

Mecp2 knockout (KO) mice—B6.129P2(C)-Mecp2tm1.1Bird/J (Jax 003890) mice were used to isolate RTT astrocytes, and crossed to Aldh1l1-eGFP mice[59]. Experimental mice came from heterozygous (+/−) Mecp2 females crossed to WT (+/y) C57BL/6J males. Astrocytes were isolated from male Mecp2 (-/y) KO mice.

Fmr1 KO mice—B6.129P2-Fmr1tm1Cgr/J (Jax 003025) mice were used to isolate FXS astrocytes, and crossed to Aldh1l1-eGFP mice[60]. Experimental mice came from

heterozygous (+/−) Fmr1 females crossed to KO (-/y) males. Astrocytes were isolated from male (-/y) and female (−/−) KO mice.

Down syndrome transgenic mice—B6EiC3Sn.BLiA-Ts(1716)65Dn/DnJ (Jax 005252) mice were used to isolate DS astrocytes, and crossed to Aldh1l1-eGFP[61,62]. Ts65Dn mice are trisomic for two-thirds of the genes orthologous to human chromosome 21 and only one copy is required, so experimental mice were generated by crossing Ts65Dn+ female mice to WT males. Trisomic genes were identified from published papers analyzing these mice[63–65]. Astrocytes were isolated from male and female Ts65Dn+ mice.

Aldh1l1-eGFP x Mecp2 KO, Fmr1 KO or Ts65Dn mice—Tg(Aldh1l1-eGFP)OFC789Gsat/Mmucd mice express Aldh1l1-eGFP in astrocytes (011015-UCD). Male Aldh1l1-eGFP mice were bred to Mecp2 or Fmr1 heterozygous (+/−) females, or Ts65Dn hemizygous females. Mecp2 and Fmr1 KO, or Ts65Dn positive male mice and their WT male littermates expressing eGFP in astrocytes were used for experiments.

Cell culture

Immunopanned cortical astrocyte cultures

Cortical mouse astrocytes were isolated by immunopanning from WT, RTT, FXS, and DS mice, by adapting a protocol for rat astrocytes[19,20]. Cortices of 2–4 mouse pups (P5-P7) were digested in papain to generate a single cell suspension, which was passed over a series of lectin or antibody-coated plates to deplete unwanted cell types (lectin [Vector Labs Inc, #L-1100] deplete endothelia; cd11b [Ebioscience, #14–01112-86] deplete microglia, cd45 [BD Pharmingen, #550539] deplete macrophages, and O4 hybridoma [see[66] for recipe] deplete oligodendrocyte precursor cells) before positive selection for astrocytes using astrocyte cell surface antigen 2 (ACSA2, Miltenyi Biotech #130–099-138). Astrocytes were plated on glass coverslips (12mm diameter, Carolina Biological Supply 633029) coated with poly-D-lysine (Sigma P6407) in 24 well plates (Falcon 353047) at 50,000–80,000 cells/well or in six well plates (Falcon 353046) coated with poly-D-lysine at 280,000 – 350,000 cells/well in growth medium containing: 50% DMEM (Thermo Fisher Scientific 11960044), 50% Neurobasal (Thermo Fisher Scientific 21103049), Penicillin-Streptomycin (LifeTech 15140–122), GlutaMax (Thermo Fisher Scientific 35050–061), sodium pyruvate (Thermo Fisher Scientific 11360–070), N-acetyl-L-cysteine (Sigma A8199), SATO (containing: transferrin (Sigma T-1147), BSA (Sigma A-4161), progesterone (Sigma P6149), putrescine (Sigma P5780), sodium selenite (Sigma S9133)), and heparin binding EGF like growth factor (HbEGF, R&D Systems 259-HE/CF). Astrocyte cultures were maintained in a humidified incubator at 37°C and 10% CO2 and grown to confluence (5–7 days).

For RNA sequencing of IP A and IP C astrocytes, at the end of the isolation procedure the cells were split in half, with half pelleted and frozen at −80C (IP acute) with the other half plated as described above and cultured for 7 days (IP cultured). At the end of the culture period the astrocytes were lifted from the plate using trypsin, pelleted and frozen at −80C until RNA extraction.

Generation of astrocyte conditioned media (ACM)

Astrocytes grown in 6 well plates had growth media removed and were washed 3 times with warm DPBS (HyClone SH30264) to remove residual protein, and placed in minimal low protein conditioning media (50% DMEM, 50% Neurobasal, penicillin-streptomycin, glutamax, sodium pyruvate, N-acetyl-Lcysteine, and carrier-free HbEGF (R&D Systems, 259-HE/CF, resuspended in dPBS with no BSA). Astrocytes were conditioned for 5 days in a tissue culture incubator at 37°C, 10% CO2. Astrocyte conditioned media (ACM) was collected and concentrated 30-fold using Vivaspin 20 or 6 centrifugal concentrators with a MW cut-off of 3 kDa (Sartorius VS2052 or VS0652). ACM protein concentration was assessed by Bradford assay (Bio-Rad 500–0006). ACM for mass spectrometry was flash-frozen with liquid nitrogen and stored at −80°C until analysis. ACM for neuronal outgrowth assays was stored at 4°C until use, for no more than 2 weeks.

McCarthy de Vellis astrocyte cultures

Astrocytes were isolated from P1 mouse cortex following the procedure of McCarthy and de Vellis as described in[18,67]. Cortices of 4 x P1 mouse pups were digested in papain, then plated in PDL coated 75cm tissue culture flasks in a serum containing medium: DMEM supplemented with 10% Heat inactivated FBS (LifeTech Cat. 10437028), Penicillin-Streptomycin, glutamax, sodium pyruvate, hydrocortisone (Sigma Cat. H0888), insulin (Sigma Cat. I1882), and N-acetyl-L-cysteine. Astrocytes form a monolayer on the bottom of the flask, and after 3 days non-adherent cells were removed by shaking the flasks; after a further 2 days the cell proliferation inhibitor AraC (10uM, Sigma C1768) was added to kill cells that divide more quickly than astrocytes e.g. microglia and OPCs. After a further 2 days the astrocyte-enriched cells were lifted from the flask using trypsin, pelleted and frozen at −80C until RNA extraction.

Immunopanned cortical neuron cultures

Cortical neurons were isolated from P5-P7 C57Bl6J WT mice using immunopanning, modified from[23]. The single cell suspension was passed over two plates to deplete unwanted cell types (lectin deplete endothelia; secondary antibody IgG H+L [Jackson Immunoresearch #115–005-167] deplete microglia) before positive selection for cortical neurons using NCAM-L1 (Millipore MAB5272). Cortical neurons were plated on glass coverslips (12mm diameter) coated with poly-D-lysine and laminin (R&D 340001001) at 10,000–20,000 cells/well in a minimal medium, with the addition of astrocyte conditioned media and/or protein factors and antibodies as described. Cortical neuron minimal media: 50% DMEM, 50% Neurobasal, Penicillin-Streptomycin, glutamax, sodium pyruvate, N-acetyl-Lcysteine, insulin, triiodo-thyronine (Sigma T6397), SATO, B27 (see[68] for recipe), and forskolin (Sigma F6886). Cortical neuron cultures were maintained in a humidified incubator at 37°C, 10% CO2.

Treatment of neurons and astrocytes with protein factors

Each neuronal experiment contained a negative control, cortical neurons in minimal media (alone condition; treated with buffer), and a positive control, cortical neurons treated with WT astrocyte conditioned media (ACM) at 3ug/mL (WT ACM condition). On rare

occasions when neurons did not display enhanced neurite outgrowth to WT ACM, that experiment was excluded from further analysis, which was a predetermined criteria. Protein treatments were Igfbp2 (R&D 797-B2 100ug/mL sterile PBS), CPE (Abcam #ab169054 100 ug/mL sterile deionized water), and BMP6 (R&D 507-BP/CF 10ug/mL sterile dPBS). Igfbp2 and CPE were applied to neurons at 4X the concentration of WT ACM (2X the concentration of ND ACM): Igfbp2=240ng/mL; CPE=160ng/mL. BMP6 was added to half the wells of WT astrocytes during the conditioning phase at 10ng/mL, a concentration determined from published research[33], and ACM collected and applied to cortical neurons at 3ug/mL. Igfbp2-neutralizing antibody (rat, R&D MAB797 at 0.5mg/mL sterile PBS) and its control IgG (rat, R&D 6–001-F at 0.5mg/mL sterile PBS) were used at 7ug/mL, twice the ND50 for Igfbp2. IGF1 (R&D 791-MG, 100ug/mL sterile PBS) was used at 100ng/mL, a concentration used in a previous study of RTT[24]. Noggin (R&D 1967-NG/CF 200ug/mL sterile PBS) was added to half the wells of FXS or RTT astrocytes during the conditioning phase at 1ug/mL and ACM collected. Due to the high levels of residual noggin in the treated ACM, FXS or RTT untreated and FXS or RTT +noggin ACM were concentrated to the same volume and a protein concentration of 3ug/mL determined in the untreated ACM; equal volumes of FXS or RTT untreated and FXS or RTT +noggin ACM were applied to cortical neurons. To test effects of noggin alone, noggin was added at 1ug/mL directly to the media immediately before plating cortical neurons.

Mass spectrometry

Protein concentration of ACM was determined by Bradford Assay and ACM was distributed into aliquots of 15ug, flash-frozen with liquid nitrogen and stored at −80°C until analysis. Samples were thawed and split into 3×5ug to produce technical triplicates for each biological replicate. Samples were precipitated by methanol/chloroform. Dried pellets were dissolved in 8M urea/100mM TEAB, pH 8.5. Proteins were reduced with 5mM tris(2-carboxyethyl)phosphine hydrochloride (TCEP, Sigma-Aldrich) and alkylated with 10mM chloroacetamide (Sigma-Aldrich). Proteins were digested overnight at 37°C in 2M urea/100mM TEAB, pH 8.5, with trypsin (Promega). Digestion was quenched with formic acid, 5% final concentration. Digested samples were analyzed on a Fusion Lumos Orbitrap Tribrid mass spectrometer (Thermo). The digest was injected directly onto a 30cm, 75um ID column packed with BEH 1.7um C18 resin (Waters). Samples were separated at a flow rate of 300nl/min on a nLC 1000 (Thermo). Buffer A and B were 0.1% formic acid in water and 0.1% formic acid in 90% acetonitrile, respectively. A gradient of 1–25% B over 160min, an increase to 35% B over 60min, an increase to 90% B over 10min and held at 100% B for a final 10min was used for 240min total run time. Column was re-equilibrated with 20ul of buffer A prior to the injection of sample. Peptides were eluted directly from the tip of the column and nanosprayed directly into the mass spectrometer by application of 2.5 kV voltage at the back of the column. The Orbitrap Fusion was operated in a data dependent mode. Full MS scans were collected in the Orbitrap at 120K resolution with a mass range of 400 to 1500 m/z and an AGC target of 4e5. The cycle time was set to 3sec, and within this 3sec the most abundant ions per scan were selected for CID MS/MS in the ion trap with an AGC target of 1e4 and minimum intensity of 5000. Maximum fill times were set to 50ms and 200ms for MS and MS/MS scans respectively. Quadrupole isolation at 1.6 m/z

was used, monoisotopic precursor selection was enabled and dynamic exclusion was used with exclusion duration of 5sec. Protein and peptide identification were done with Integrated Proteomics Pipeline – IP2 (Integrated Proteomics Applications). Tandem mass spectra were extracted from raw files using RawConverter[69] and searched with ProLuCID[69] against Uniprot mouse database. The search space included all fully-tryptic and half-tryptic peptide candidates, carbamidomethylation on cysteine was considered as a static modification.

The validity of the peptide spectrum matches (PSMs) generated by ProLuCID was assessed using Search Engine Processor (SEPro) module from PatternLab for Proteomics platform[70]. XCorr, DeltaCN, DeltaMass, ZScore, number of peaks matched, and secondary rank values were used to generate a Bayesian discriminating function. A cutoff score was established to accept a false discovery rate (FDR) of 1% based on the number of decoys. A minimum sequence length of six residues per peptide was required and results were post-processed to only accept PSMs with < 10ppm precursor mass error. We performed a pairwise comparison of each individual ND versus WT using PatternLab's TFold module. The following parameters were used to select differentially expressed proteins: spectral count data were normalized using NSAF values[71], and two nonzero replicate values were required for each condition. A BH q-value was set at 0.05 (5 % FDR). A variable fold-change cutoff for each individual protein was calculated according to the t-test p-value using an F-Stringency value automatically optimized using the TFold module.

qRT-PCR & RNA sequencing of immunopanned ND astrocytes

For qRT-PCR RNA was collected using the RNEasy Micro Plus kit (Qiagen 74034). Aliquots (0.1 – 0.5 ug) of RNA were used for cDNA synthesis using Superscript VILO master mix (Thermo Fisher Scientific 11755050). An equal amount of whole brain RNA from a mouse with matching genotype (WT, Mecp2 KO, Fmr1 KO, or Ts65Dn Mut) was used to generate control whole brain cDNA. 1 uL of cDNA was used for qPCR reaction using SYBR green PCR mastermix (Life Supply 4309155). All samples were run in triplicates (technical replicates). Primer pairs: GAPDH (loading control; forward TGCCACTCAGAAGACTGTGG, reverse GCATGTCAGATCCACAATGG); Syt1 (neurons; forward CTGCATCACAACACTACTAGC, reverse CCAACATTTCTACGAGACACAG); GFAP (astrocytes; forward AGAAAACCGCATCACCATTC, reverse TTGAGAGGTCTTGTGACTTTT); CSPG4 (oligodendrocyte precursor cells; forward CTCAGAACCCTATCTTCACG, reverse TACATGGTAGTGGACCTCAT); CD68 (microglia; forward ATACAATGTGTCCTTCCCAC, reverse CTATGCTTGCATTTCCACAG); FGFR4 (fibroblasts; forward AGAGTGACGTGTGGTCTTT, reverse ACTCCCTCATTAGCCCATAC). Only samples that had GFAP expression of ≥3x whole brain and CSPG4 expression of ≤2x whole brain were used for proteomics and gene expression analysis.

For RNA sequencing ND astrocytes RNA was collected using the RNEasy Micro Plus kit (Qiagen 74034). RNA libraries were prepared with TrueSeq Stranded mRNA Library Prep Kit (Illumina), from an average 0.8ug total RNA. Poly(A) mRNA was isolated from total RNA samples, followed by mRNA fragmentation, first strand cDNA synthesis, second

cDNA synthesis and adaptor ligation, and isolation and amplification of cDNA fragments. Illumina HiSeq 2500 instrument was used for sequencing, with a read length of 50bp single-end, and an average of 36 million reads per sample. For RNA sequencing IP A, IP C and MD C astrocytes, mRNA was isolated from pelleted cells using the RNeasy Mini Plus kit (Qiagen 74134). RNA libraries were prepared with TrueSeq Stranded mRNA Library Prep Kit (Illumina) from 0.5ug total RNA. Poly(A) mRNA was isolated from total RNA samples, followed by mRNA fragmentation, first strand cDNA synthesis, second cDNA synthesis and adaptor ligation, and isolation and amplification of cDNA fragments. Illumina HiSeq 2500 instrument was used for sequencing, with a read length of 50bp single-end, and an average of 40 million reads per sample.

Sequenced reads were quality-tested using FASTQC v0.11.8 and aligned to the mm10 mouse genome using the STAR aligner version 2.5.3a. Mapping was carried out using default parameters, filtering non-canonical introns and allowing up to 10 mismatches per read and only keeping uniquely mapped reads. The genome index was constructed using the gene annotation supplied with the mm10 Illumina iGenomes collection and sjdbOverhang value of 100. Raw or FPKM (fragments per kilobase per million mapped reads) gene expression was quantified across all gene exons with HOMER v4.10.4 analyzeRepeats.pl with mm10 annotation v5.10 and parameters -strand + -count exons -condenseGenes (top-expressed isoform as proxy for gene expression), and differential gene expression was carried out on the raw counts with HOMER getDiffExpression.pl that runs DESeq2 v1.14.1 using replicates to compute within-group dispersion. BMP6 treatment samples were adjusted for replicate-specific batch effects using the -batch flag. Differentially expressed genes were defined as having FDR<0.05, FC>1.5, and FPKM>1, when comparing two experimental conditions. Pathway analysis was performed using PANTHER v13, using the over-representation test with Fisher's Exact test and false discovery rate corrected[72].

Immunocytochemistry

Staining astrocytes for cell-specific markers

After 7 days (astrocytes not treated with additional factors) or 12 days (astrocytes conditioned with BMP6 or noggin), astrocytes were fixed with warm (37°C) 4% paraformaldehyde (PFA; EMS 50980487) for 20 minutes. Coverslips were washed 3x with room temperature (RT) PBS and blocked and permeabilized for 30 minutes in 50% goat serum/50% antibody buffer (150 mM NaCl; 50 mM Tris; 100 mM L-lysine; 1% BSA; pH 7.4) and 0.5% Triton X-100 (Sigma T9284). Coverslips were washed 1x with PBS and incubated overnight at 4°C with primary antibodies against GFAP (1:1000, mouse, Millipore, MAB360), Aqp4 (1:1000, rabbit, Sigma, A5971), GLAST (1:100, mouse, Miltenyi 130–095-822), NeuN (1:1000, mouse, Millipore, MAB377), Iba1 (1:1000, rabbit, Wako, 016–20001), or NG2 (1:1000, rabbit, Millipore, AB5320) in a solution of antibody buffer + 10% goat serum. The following day cells were washed 3x with PBS and incubated for 2 hours with appropriate secondary antibodies (goat anti-rabbit Alexafluor 594 (1:1000, Thermo Fisher Scientific A-11037), goat anti-mouse Alexafluor 488 (1:1000, Thermo Fisher Scientific A-11029), goat anti-mouse Alexafluor 594 (1:1000, Thermo Fisher Scientific A-11032)) in a solution of antibody buffer + 10% goat serum, before being washed

3x and mounted with SlowFade + DAPI (Life Technologies s36939) on glass slides (Fisherfinest 12–244-2) and sealed with clear nail polish (Electron Microscopy Sciences 72180). Astrocytes were imaged using a Zeiss Axio Imager Z2 motorized microscope (430000–9902) using a 20X 0.8NA objective and Zeiss Axiovision software. Images were analyzed using ImageJ by calculating the % of total cells (DAPI) that were positive for the cell marker.

Neurite staining of cortical neurons

After 48 hours in culture cortical neurons were fixed for 10 minutes with 4% PFA at 37°C. Coverslips were washed 3x with RT PBS and blocked and permeabilized for 30 minutes in 50% antibody buffer/50% goat serum and 0.5% Triton X-100. Coverslips were washed 1x with PBS and incubated overnight at 4°C with primary antibodies against MAP2 (to mark dendrites) (1:5000, chicken, EnCor Biotechnologies CPCA-MAP2) and Tau (to mark axons) (1:500, mouse, Millipore Sigma MAB3420) in a solution of antibody buffer + 10% goat serum. The following day, cells were washed 3x with PBS and incubated for 2 hours with secondary antibodies (goat anti-chicken Alexafluor 488 (1:1000, Thermo Fisher Scientific A11039), goat anti-mouse Alexafluor 594 (1:1000)) in a solution of antibody buffer + 10% goat serum, then washed 3x with PBS and mounted with SlowFade + DAPI on glass slides, sealed with nail polish. Cortical neurons were imaged using a 10X 0.45NA objective on a Zeiss Axio Imager microscope. Imaging for each assay: 3 coverslips/condition, 20 images/coverslip, total of 60 images per condition per assay with at least 1 neuron per image. Images were processed in ImageJ to merge all channels, convert the images to 16-bit, and apply a normalization of 0.1. Analysis for Figures 1i, 4e, 5b,d,f, 7e,i: Images were analyzed using MetaMorph software (Molecular Devices), using the Neurite Outgrowth Module to measure total, mean, max, and median neurite outgrowth length, number of processes per cell. Analysis for Figures 7f,j: Images were analyzed using the NeuronJ Plugin for Image J to measure total outgrowth per cell.

Cortical neuron layer marker immunostaining

Cortical neurons were cultured and fixed as described in the neurite staining section. All coverslips were incubated with primary antibody against MAP2 and a cell-type marker: Satb2 (1:500, rabbit, Abcam Ab92446), Ctip2 (1:500, rat, Abcam Ab18465), Tbr1 (1:500, rabbit, Abcam Ab31940), Reelin (1:500, mouse, Abcam Ab78540), GAD (1:1000, mouse). Secondary antibodies were used at 1:1000: goat anti-chicken Alexafluor 488, goat anti-mouse Alexafluor 594, goat anti-rabbit Alexafluor 594 and goat anti-rat Alexafluor 594 (Thermo Fisher A11007). Cortical neurons were imaged using a 20X (0.8NA) objective on a Zeiss Axio Imager microscope. Cells were selected for imaging by being immunopositive for MAP2. Imaging for each assay: 3 coverslips/condition, 20 images/coverslip, total of 60 images per condition per assay with at least 1 neuron per image. The percentage of MAP2 positive cells immunopositive for the marker was calculated by visual inspection of each image in Image J.

Immunohistochemistry and in situ hybridization

Tissue collection and preparation

P7 male littermate mice were used (Aldh1l1-eGFP;Mecp2-/y and Aldh1l1-eGFP;Mecp2+/y; Aldh1l1-eGFP;Fmr1-/y and Aldh1l1-eGFP;Fmr1+/y; Aldh1l1-eGFP;Ts65Dn+ve and Aldh1l1-eGFP;Ts65Dn-ve). Mice were anesthetized with intraperitoneal injection of 100mg/kg Ketamine (Victor Medical Company) and 20mg/kg Xylazine (Anased) mix and transcardially perfused with PBS followed by 4% PFA. Brains were dissected and postfixed in 4% PFA at 4°C overnight, washed 3x in PBS and cryoprotected in 30% sucrose at 4°C for 48 hours, then frozen in TFM (General data healthcare TFM-5) in a dry ice/ethanol mix and stored at −80°C.

Immunohistochemical staining for Igfbp2 and pSMAD in P7 mouse brains

Coronal sections containing the visual cortex were collected on Superfrost Plus micro slides (VWR 48311–703) at 14um thickness (3.4 mm posterior to Bregma) on a cryostat (Hacker Industries OTF5000). Sections were blocked and permeabilized for 1hr at RT in antibody buffer + 0.3% Triton X-100. Primary antibodies, goat anti-Igfbp2 (1:500, R&D AF797) or rabbit anti-pSMAD (1:800, Cell Signaling 9516), were incubated in antibody buffer + 0.3% Triton X-100 overnight at 4°C. Slices were washed 3x with PBS and incubated for 2hr at RT with appropriate secondary antibody, donkey anti-goat Alexafluor 594 (1:500, Thermo Fisher Scientific A-11058) or goat anti-rabbit Alexafluor 594 (1:500) in antibody buffer + 0.3% Triton X-100. Sections were washed 3x with PBS and mounted with SlowFade gold antifade mountant with DAPI. Coverslips (22 mm x 50 mm 1.5 thickness (Fisher Scientific 12–544-D)) were placed on top of sections and sealed with clear nail polish. Negative controls included sections where Igfbp2 or pSMAD primary antibodies were omitted.

For Igfbp2 layer 2/3 of visual cortex was imaged using a Zeiss LSM 880 Rear Port Laser Scanning Confocal Microscope with Zen Black software. Images were taken using a 63X objective, as 16 bit images and z-stacks of 10 steps with a total thickness of 3.85um. Acquisition settings were the same for WT and KO/TG samples imaged in the same experiment (littermate pairs). Imaging was performed on 3 sections (technical replicates) from 6 or 7 mice (biological replicates) per genotype. Analysis was performed using IMARIS software (Bitplane). Astrocytes (eGFP) were defined as surfaces with background subtraction (largest sphere contained within the surface set to 5um) and smoothed to 0.110um. Igfbp2 (channel 594) was masked within and without these surfaces to allow separate analysis of internal and external Igfbp2, which was also defined as surfaces. The investigator was blinded to the genotypes of the mice during sectioning, staining, imaging, and analysis. Representative images are maximum intensity projections of the z-stack image.

For pSMAD all layers of the visual cortex were imaged using a Zeiss LSM 880 Rear Port Laser Scanning Confocal Microscope. Images were acquired using a 20X objective, as 16 bit images of 4–6 tiles with 10% overlap, z-stacks of 3 steps with a total thickness of 2.27um. Imaging was performed on 3 sections (technical replicates) from 3 mice (biological replicates) per genotype. Maximum intensity projections were generated in Zen Black and exported as TIFF images for analysis in ImageJ. ROIs of 1800 × 1200 pixels were made

to encompass layers I-IV of the cortex, and expression of pSMAD in the nucleus measured using the particle analysis tool in ImageJ and counted using the Cell Counter plugin. DAPI was used to create a mask, and proportion of pSMAD positive astrocytes was determined by counting the number of colocalized DAPI+ pSMAD+ eGFP+ cells and normalizing to total number of astrocytes. The investigator was blinded to the genotypes of the mice during sectioning, staining, imaging, and analysis.

Single-molecule fluorescent in situ hybridization (smFISH) to detect Igfbp2 mRNA

smFISH RNAscope experiments were performed on P7 Aldh1l1-eGFP brains fixed with 4% PFA and processed as described in the Tissue Collection section. Sagittal sections containing the primary visual cortex were made at 14um using a cryostat. The assay was performed with the RNAscope 2.5 HD—Fluorescent Multiplex Manual Assay kit (ACDbio #320850) using manufacturer's instructions for fixed-frozen tissue with modifications, as reported in[73]. Following cryosectioning slides were washed for 5 min in PBS at RT, followed by brief wash (~1min) in 100% Molecular Biology Grade Ethanol. Slides were air-dried for 5min, incubated with protease 3 at 40C for 30min. Slides were then briefly washed with PBS and incubated with target probes (Igfbp2 #405951 and either NG2/Cspg4 #404131-C3 or Tubb3 #423391-C3) for 2 hrs at 40C, followed by 3 amplification steps and 1 detection step. Slides were stained with chicken anti-GFP (1:500, Millipore 06–896) and goat anti-chicken Alexafluor 488 (1:500), following procedure described in Immunohistochemical Staining section. DAPI-containing mounting media was applied and slides were coverslipped and sealed with nail polish.

Slides were imaged using Zeiss LSM 700 confocal microscope with Zen software at 40X magnification. An 1926×2868 pixel z-stack image was obtained (pixel size 0.16 × 0.16 × 0.4 μm, 12 slices per 4.4 μm stack, 16 bit images of 6 tiles with 10% overlap) encompassing cortical layers 1 through 3. Imaging was performed on 3 sections (technical replicates) from 3 mice (biological replicates) for each pair of probes. Example images show maximum intensity projections with both pairs of probes. Analysis was performed in ImageJ, as described in[73]. Astrocytes were identified using the GFP signal, and neurons and NG2 cells were identified using the Tubb3 and Cspg4 probe signals respectively. An ROI outline was created around the cell body and primary processes of each cell. The Igfbp2 probe signal was thresholded in the same way for all images, and the thresholded area was recorded for each cell.

Analysis of cell body size in RTT

Neurons in the visual cortex were labeled with GFP by injecting mice at P2 with AAV8-hSyn-EGFP (AAV-synapsin-GFP), and brains collected at P7 for analysis. pAAV-hSyn-EGFP was a gift from Bryan Roth (Addgene viral prep # 50465-AAV8; RRID:Addgene_50465). P2 mice were anesthetized by chilling and injected on a stereotaxic frame (Kopf# 940) equipped with a Nanoject III (Drummond #3–000-207), with injection coordinates 1.5mm dorsal and 0.6mm anterior from lambda. 500nl of virus was injected at two depths (250 and 150μm) from the surface of the skull at a total titer of 2×10^8 vg and a speed of 50nl/sec. For RTT analysis injections were performed on littermate pairs of male Mecp2+/y (WT) and Mecp2-/y (RTT) mice. For Igfbp2 blocking antibody experiments

injections were performed on littermate pairs of male Mecp2-/y (RTT) mice, receiving either the Igfbp2 blocking antibody (R&D MAB797) or the isotype control antibody (R&D 6–001-F) at 1mg/ml in PBS, labeled with Alexafluor 594 to visualize the injection site (Molecular Probes A20185), with the AAV-Synapsin-GFP virus diluted in the antibody solution.

Brains were collected and processed as described in the Tissue Collection and Immunohistochemistry sections. Coronal sections were obtained on a cryostat at 60μm, mounted and coverslipped, and imaged on an upright fluorescence Zeiss Axio Imager. Z-stack images were taken of the full section thickness, 0.5 μm step size, using a 20X air objective (NA 0.8) and an ApoTome.2 for optical sectioning. A minimum of 3 sections (technical replicates) per mouse were imaged. In cases where the full width of the cortex did not fit within the imaging window, separate images of upper and deep layer neurons were obtained. Maximum intensity projections were generated in Zeiss Zen software. Analysis was performed in Image J - for upper layer neurons analysis was restricted to cells within 150um of the bottom of layer 1; for deep layer neurons the neuronal layer was identified by the presence of neurons with characteristically large cell bodies present in layer 5. Neurons with an obvious dendritic protrusion were identified and the area of the cell body measured by manually tracing the outline of the cell body. Image analysis was performed blind to genotype. The same analysis procedure was applied to neurons in vitro.

Experimental Design, Statistical Analysis and Data Presentation

No statistical methods were used to pre-determine sample sizes but our sample sizes are similar to those reported in previous publications[4,12,13,16,17,34,46,55]. Mice were assigned to groups based on genotype; they were randomly numbered prior to genotyping and paired for experiments with their nearest numbered opposite genotyped sibling to create wild-type and knock-out/transgenic pairs. Samples were imaged in numerical order, regardless of genotype, which served to randomize the imaging order. For generating *in vitro* astrocytes, mutant mice in the litter were collected in numerical order until the maximum 4 mice per litter was reached. For *in vivo* experiments in Figure 4&6, after animals were genotyped and pairs were determined, the researcher retained genotyping information in a digital file and did not include the genotypes on the samples throughout the tissue preparation, staining, imaging, and analysis process; in processing multiple pairs of animals. For experiments in Figure 5 a separate experimenter collected the images, and the analyzer was blinded to genotype/treatment. For *in vitro* experiments the experimenter was not blinded to condition. Statistical tests were performed using Graphpad Prism 9. All tests are two-tailed. Data was first tested for normality of distribution. For normally distributed data student's t-test was used for two groups, and for more than two groups one-way ANOVA with Dunnett's post hoc test for multiple comparisons. For non-normally distributed data multiple comparisons were done by Kruskal-Wallis ANOVA on ranks and two groups were compared with Mann-Whitney Rank Sum test. Statistical test used and exact p-values are reported on graphs, in figure captions, and provided as source data files. Graphs and heatmaps were generated using Prism 9. For analysis of neurons in vitro, data is presented from all cells and the number of cells indicated in the figure legend. In the main figures data is presented as violin plots, with the dashed line marking the median and dotted lines marking the 25th and 75th percentile; in the supplementary figure the same data is represented as a cumulative

distribution plot. For analysis of in vivo changes, data is averaged from each mouse, and data points on bar graphs represent individual mice. Proportional Venn diagrams were generated using Biovenn http://www.biovenn.nl/index.php. Schematics were generated using Biorender.

Data Availability

RNA sequencing raw data has been deposited in GEO, GSE139285. https://www.ncbi.nlm.nih.gov/geo/. The mass spectrometry proteomics data have been deposited to the ProteomeXchange Consortium via the PRIDE partner repository with the dataset identifier PXD015996, https://www.ebi.ac.uk/pride. Source data that supports all findings in the study are available as supplemental tables (proteomics and RNA sequencing) and source data tables (statistical analysis). The data that support this study are available from the corresponding author upon reasonable request.

Code Availability

No new code was used in this study

Extended Data

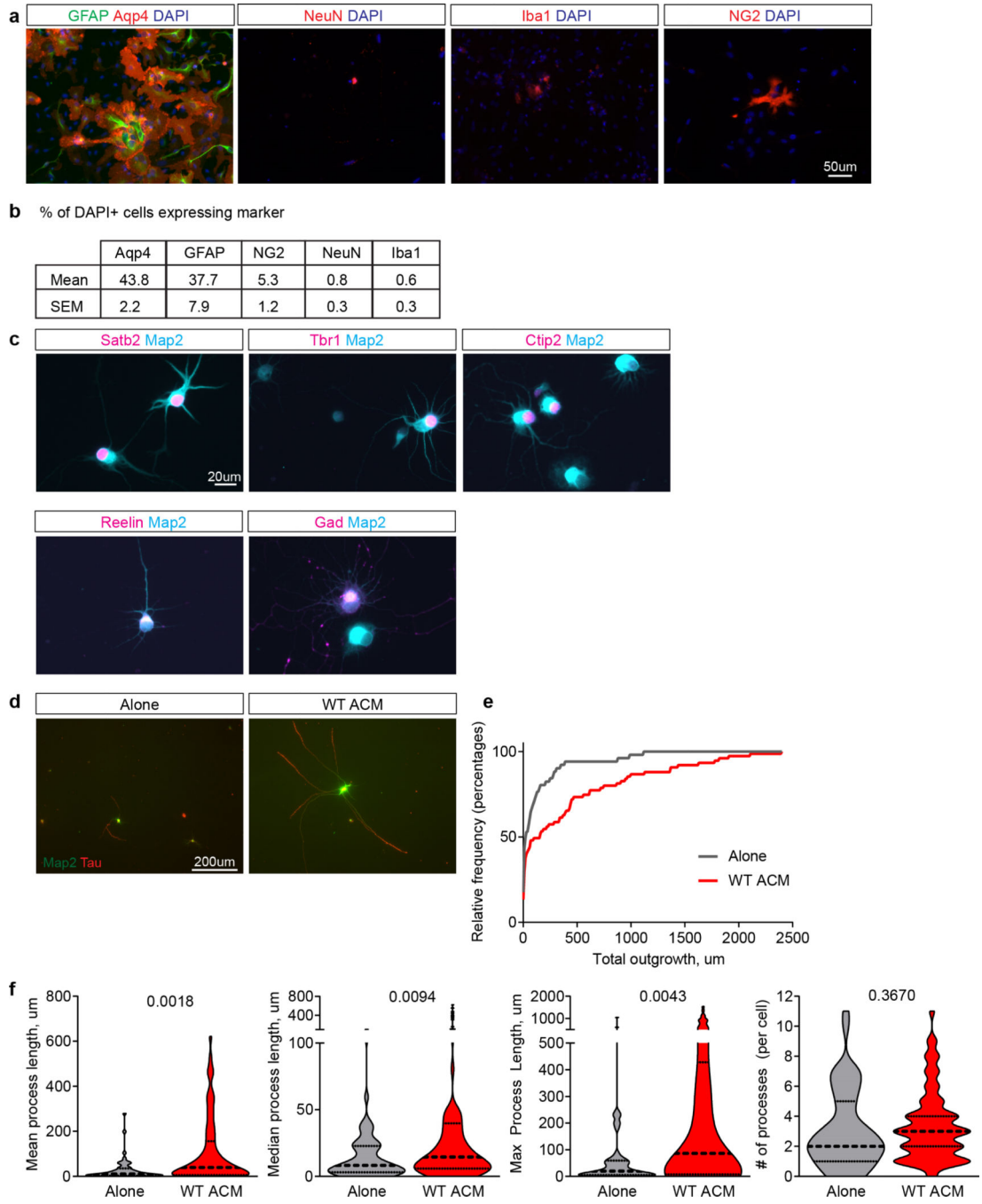

	Aqp4	GFAP	NG2	NeuN	Iba1
Mean	43.8	37.7	5.3	0.8	0.6
SEM	2.2	7.9	1.2	0.3	0.3

Extended Data Fig. 1. Immunopanned astrocyte and neuron cultures for study of NDs.

a,b. Immunostaining IP-astrocyte cultures for cell type markers reveals that the majority of cells express astrocyte-associated proteins Gfap and Aqp4, while rarely expressing NeuN (neuronal marker), Iba1 (microglial marker) or NG2 (oligodendrocyte precursor cell marker), N=15 experiments (3WT, 1 RTT, 3 FXS, 8 DS; no differences were observed between ND and WT expression of cell markers). **c.** Example images of WT immunopanned

neurons cultured for 2 days in WT ACM, and immunostained for MAP2 to identify neurons and antibodies against cortical neuron layer-enriched marker genes. Data analyzed in Figure 1g. N=3 experiments SATB2, TBR1, CTIP2; N=4 Reelin; N=2 GAD. **d.** Example images from Figure 1h, prior to processing and analysis. WT neurons immunostained with MAP2 (dendrites, green) and tau (axon, red). **e.** Relative frequency of total neurite outgrowth, example experiment shown, same data as Figure 1i. **f.** Examination of additional measures of neurite growth for experiments in Figure 1h,i. Violin plot: dashed line median, dotted lines 25^{th} and 75^{th} percentile. Number of neurons: alone = 51, WT ACM = 75. Statistics by 2-sided Mann-Whitney test.

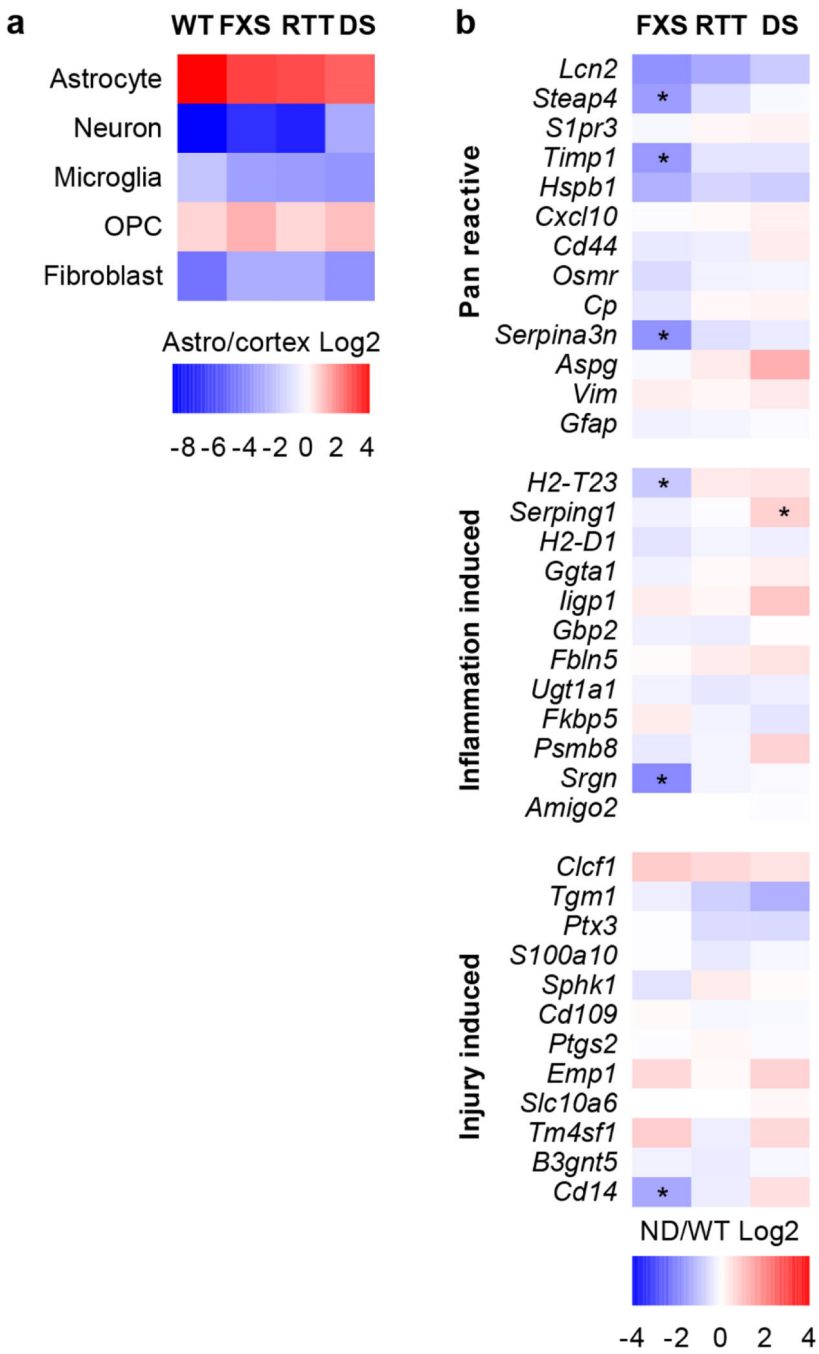

Extended Data Fig. 2. IP astrocytes reproduce in vivo alterations to ND astrocytes.

a. qRT-PCR for cell-type markers from mRNA collected from IP astrocytes compared to P7 mouse cortex demonstrates enrichment for astrocytes (Gfap), a depletion of neurons (Syt1), microglia (Cd68), fibroblasts (Fgfr4), and a decrease in oligodendrocyte precursor cells (OPCs; Cspg4) in WT and ND IP astrocyte cultures. N=6 cultures per genotype. WT data same as in Figure 1b. **b.** Reactive astrocyte markers from pan reactive, inflammation-induced and injury-induced reactive astrocytes are not consistently altered in IP astrocyte cultures from ND compared to WT, demonstrating cultures are not reactive. Data from

RNA sequencing. N=6 cultures WT, RTT, FXS; 4 DS. *adjusted p<0.05, FPKM>1 and fold change ≥1.5 calculated with DESeq2.

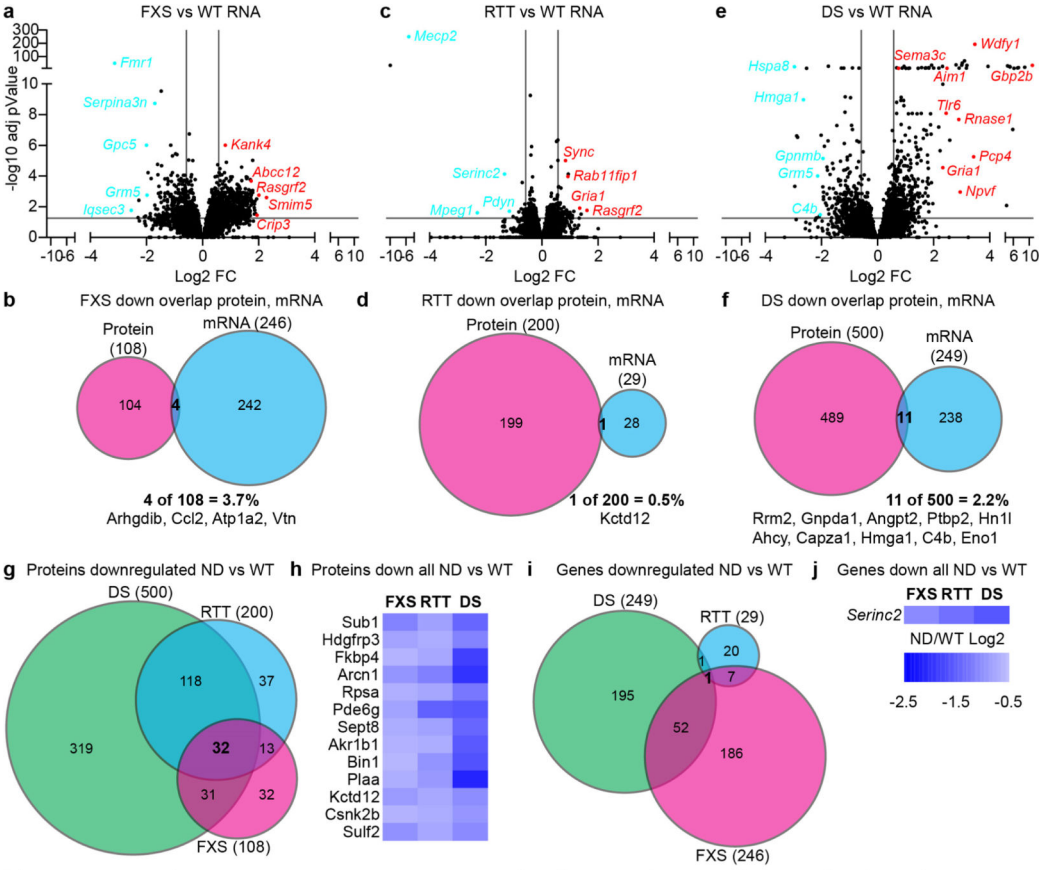

k

PROTEIN DOWN - PANTHER Pathways	FXS (FDR)	RTT (FDR)	DS (FDR)	ND (FDR)
Parkinson disease (P00049)	n/a	n/a	3.27E-09	n/a
Huntington disease (P00029)	n/a	n/a	2.24E-09	n/a

PROTEIN DOWN - Reactome pathways	FXS (FDR)	RTT (FDR)	DS (FDR)	ND (FDR)
Ion homeostasis (R-MMU-5578775)	2.01E-02	n/a	n/a	n/a
Signaling by Hedgehog (R-MMU-5358351)	n/a	n/a	3.91E-15	n/a

RNA UP - Reactome pathways	FXS (FDR)	RTT (FDR)	DS (FDR)	ND (FDR)
Cilium Assembly (R-MMU-5617833)	3.94E-06	n/a	n/a	n/a
Organelle biogenesis and maintenance (R-MMU-1852241)	1.28E-05	n/a	n/a	n/a

RNA DOWN - PANTHER Pathways	FXS (FDR)	RTT (FDR)	DS (FDR)	ND (FDR)
Cadherin signaling pathway (P00012)	2.58E-02	7.96E-19	n/a	n/a
Wnt signaling pathway (P00057)	7.04E-03	2.14E-15	n/a	n/a
p53 pathway (P00059)	n/a	n/a	3.48E-03	n/a
Endogenous cannabinoid signaling (P05730)	3.95E-02	n/a	n/a	n/a
Metabotropic glutamate receptor group I pathway (P00041)	4.05E-02	n/a	n/a	n/a

RNA DOWN - Reactome pathways	FXS (FDR)	RTT (FDR)	DS (FDR)	ND (FDR)
Extracellular matrix organization (R-MMU-1474244)	1.23E-03	n/a	2.68E-05	n/a
ADP signalling through P2Y purinoceptor 1 (R-MMU-418592)	3.25E-02	n/a	n/a	n/a
GABA synthesis, release, reuptake, degradation (R-MMU-888590)	n/a	n/a	4.50E-02	n/a

Extended Data Fig. 3. Altered protein secretion and gene levels of ND astrocytes.

a,c,e. Volcano plot of genes expressed by astrocytes at FPKM >1, plotted as Log2FC against -log10 p-value comparing each disorder to WT: FXS (**a**), RTT (**c**) and DS (**e**). Each dot represents a gene; top right sector genes significantly upregulated (FC>1.5, adjusted p-value <0.05), examples in red; top left sector genes significantly downregulated

(FC<−1.5, adjusted p-value <0.05), examples in turquoise, calculated with DESeq2. **b,d,f.** Venn diagram of overlap between proteins and genes with decreased level in FXS (**b**), RTT (**d**) and DS (**f**) ACM and astrocytes **g,h.** Venn diagram showing overlap in proteins downregulated in all ND (**g**), and heatmap of top altered proteins ranked by abundance in WT ACM (**h**). **i,j.** Venn diagram showing number of genes downregulated (**i**) and corresponding heatmap (**j**) of overlapping altered genes. Scale bar in **j** also applies to heatmap in **h**. **k.** Pathway analysis of proteins and genes altered in ND astrocytes compared to WT demonstrates some overlapping and some unique alterations in ND astrocyte function compared to WT, performed using PANTHER over-representation test with Fisher's Exact test and FDR corrected. Proteomics, N=6 cultures per genotype, $p<0.05$, abundance >0.01%, fold change between WT and ND ≥1.5. RNASeq, N=6 cultures WT, RTT, FXS; 4 DS, adjusted $p<0.05$, FPKM>1, fold change between ND and WT ≥1.5.

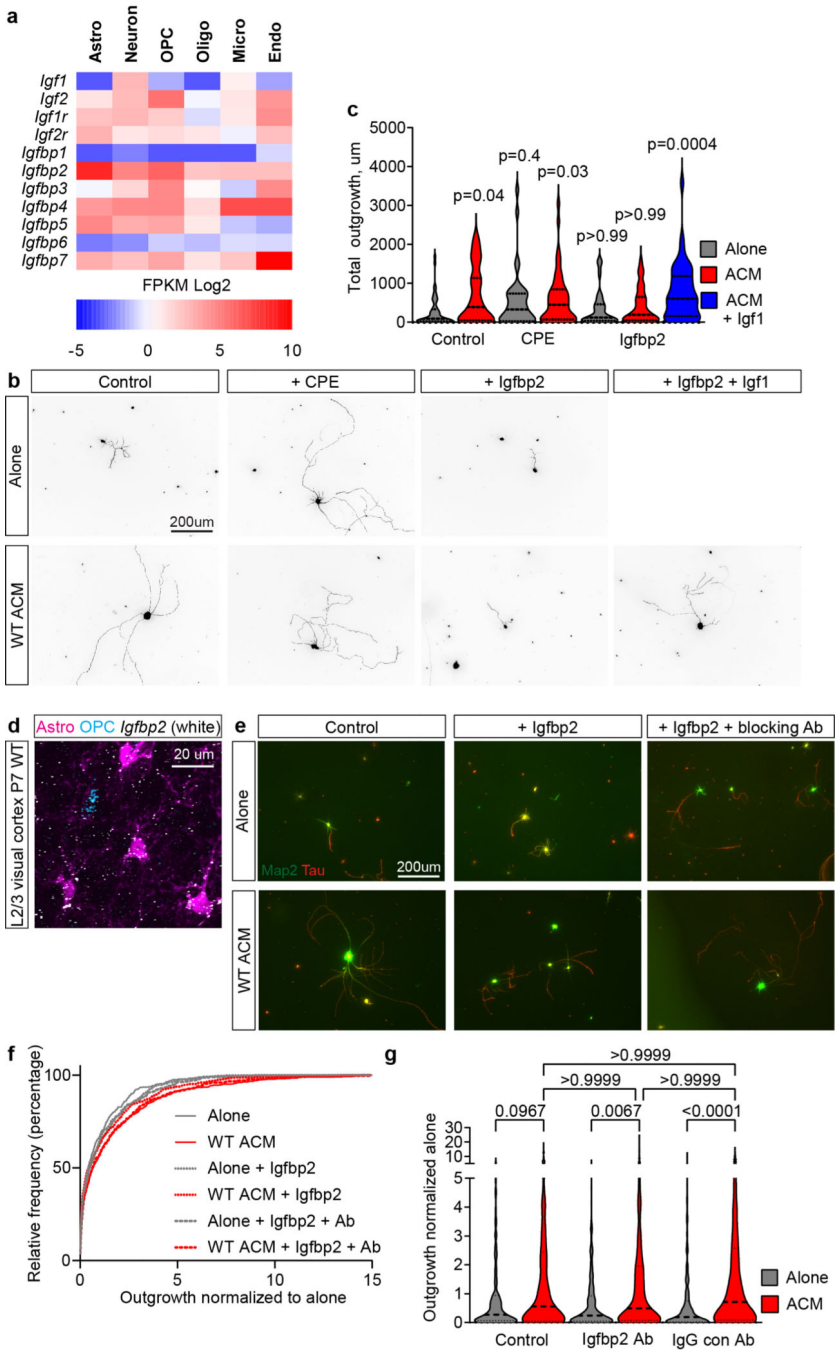

Extended Data Fig. 4. Excess Igfbp2 in ACM inhibits neurite outgrowth.

a. Expression of IGF family members in cortical cell types (data from Zhang et al., 2014). **b,c.** Addition of Igfbp2 protein to WT ACM inhibits WT neurite outgrowth, which is reduced by adding IGF1. Addition of CPE protein to WT ACM does not inhibit WT neurite outgrowth. **b.** Example images of WT neurons cultured for 48 hours, conditions as marked (image merge of MAP2 + Tau). **c.** Quantification of total neurite outgrowth. Example experiment shown, repeated 2 times with same result, number of neurons: control alone=49, control ACM=50, CPE alone=36, CPE ACM=46, Igfbp2 alone=44, Igfbp2 ACM=48, Igfbp2

ACM + Igf1=39. **d.** smFISH against Igfbp2 mRNA in the P7 visual cortex in Aldh1l1-GFP mice to mark astrocytes, combined with probe for OPCs (Cspg4). See Figure 4g for quantification. N=3 WT mice. **e.** Example images from Figure 4d prior to processing and analysis. Neurons immunostained with MAP2 (dendrites, green) and tau (axon, red). **f**. Relative frequency distribution plot of total neurite outgrowth length, pooled data from 3 experiments, same data as Figure 4e. **g.** Adding the IgG control antibody to WT ACM does not alter neurite outgrowth. Example experiment shown, repeated twice with same result. Number of neurons: control alone=216, control ACM=333, Igfbp2-Ab alone=257, Igfbp2-Ab ACM=267, IgG con-Ab alone=277, IgG con-Ab ACM=266. Violin plots (**c,g**), dashed line marks median, dotted lines 25^{th} and 75^{th} percentile. Statistics by Kruskal-Wallis one-way ANOVA on ranks with Dunn's test for multiple comparisons, p values compared to control alone condition (**c**).

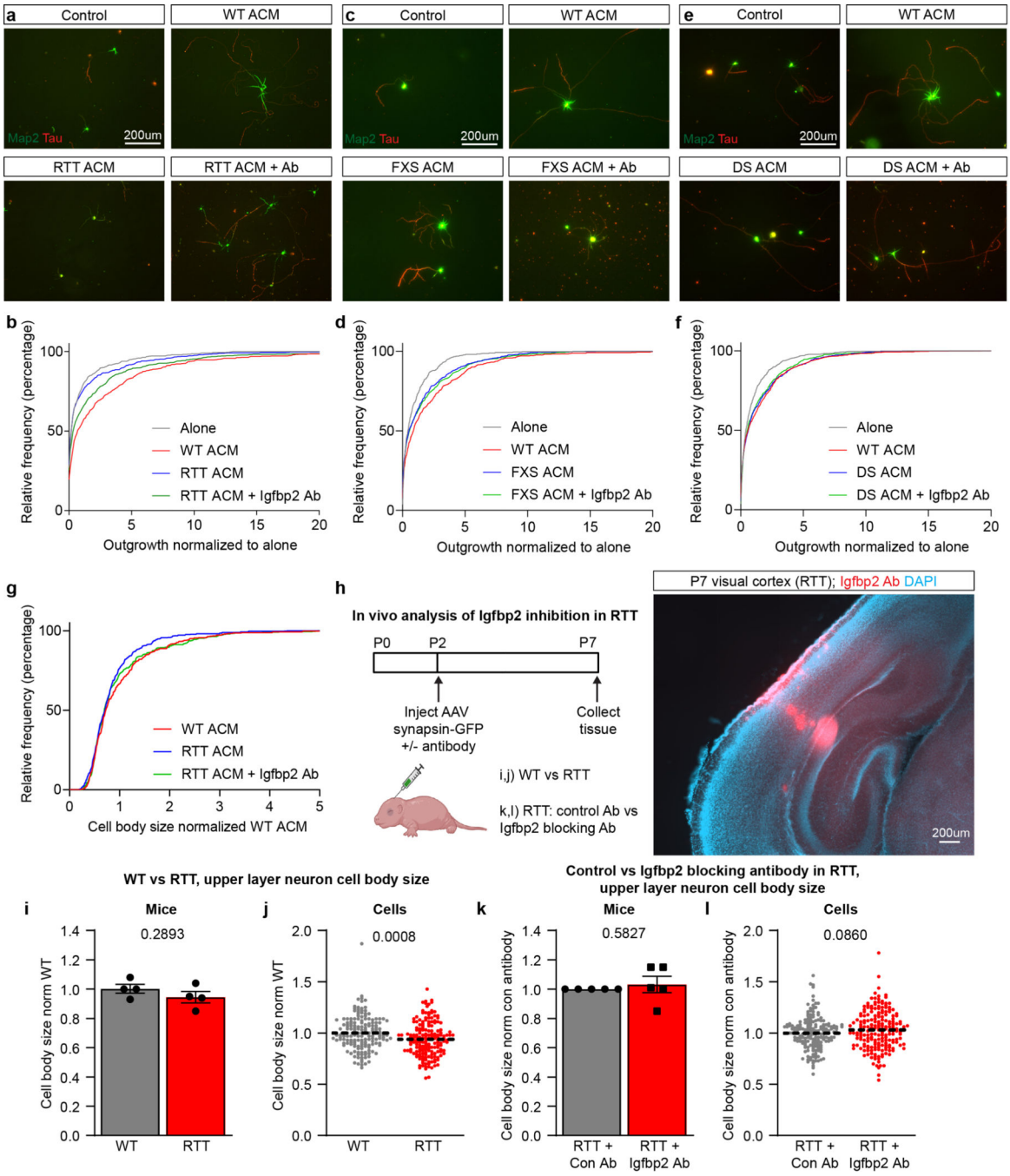

Extended Data Fig. 5. Blocking Igfbp2 in RTT reduces neural developmental deficits.

a,c,e. Example images from Figure 5a,c,e prior to processing and analysis. Neurons cultured for 48 hours in RTT (**a**), FXS (**c**) or DS (**e**) ACM and immunostained with MAP2 (dendrites, green) and tau (axon, red). **b,d,f**. Relative frequency distribution plot of total neurite outgrowth, pooled data from 3 (**b**), 4 (**d**), 5 (**f**) experiments per graph, same data as Figure 5b,d,f. Number of neurons: RTT (**b**): alone=439, WT ACM=549, RTT ACM=633, RTT ACM + Igfbp2-Ab=621; FXS (**d**): alone=492, WT ACM=608, FXS ACM=621, FXS ACM + Igfbp2-Ab=647; DS (**f**): alone=716, WT ACM=992, DS ACM=765, DS ACM + Igfbp2-

Ab=858. **g.** Relative frequency distribution plot of neuronal cell body size, pooled data from 3 experiments, same data as Figure 5g. **h-l** Cell body size of upper layer cortical neurons is not different between WT and RTT mice, and unaffected by the Igfbp2 neutralizing antibody. **h.** Schematic of the experiment: P2 mice were injected in the visual cortex with AAV synapsin-GFP +/− antibody, and tissue collected at P7 and GFP-expressing neurons imaged, with the region to be imaged identified by the presence of the fluorescently labeled antibody. **i,j.** Cell body area in upper layer neurons is unaltered in RTT compared to WT mice. **i.** Analysis by mice, graph average ± s.e.m., individual data points represent mice, N = 4 WT and 4 RTT mice, statistics by 2-sided T-test. **j.** Analysis by cells, graph individual data points represent cells, dashed line represents the mean, n = 162 WT and 177 RTT cells, statistics by 2-sided T-test. **k,l.** Cell body area in upper layer neurons in RTT mice is unaffected by an Igfbp2 neutralizing antibody. **k.** Analysis by mice, graph average ± s.e.m., individual data points represent mice, N = 5 control-Ab and 5 Igfbp2-Ab mice, statistics by 2-sided T-test. **l.** Analysis by cells, graph individual data points represent cells, dashed line represents the mean, n = 183 control-Ab and 195 Igfbp2-Ab cells, statistics by 2-sided T-test.

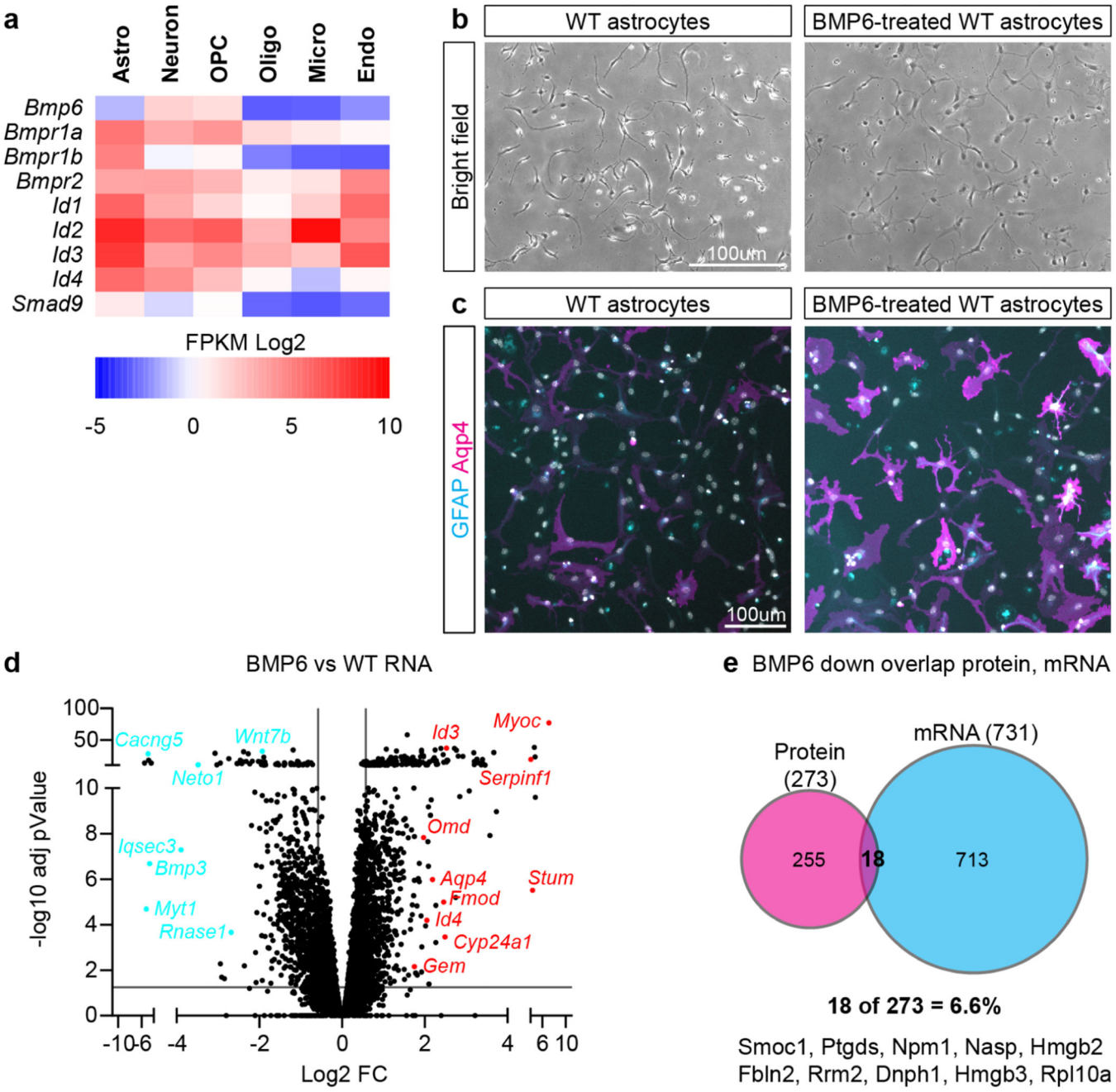

Extended Data Fig. 6. Activating WT astrocyte BMP signaling mimics ND astrocytes.

a. Relative expression of BMP family members in purified cell types in the cortex shows enrichment for BMP target genes in astrocytes (data from Zhang et al, 2014). **b,c**. BMP6-treated astrocytes have thinner more branched processes (**b**), and increased expression of both GFAP (cyan) and AQP4 (magenta) (**c**). Example images shown, experiment repeated 3 times with same effect. **d.** Volcano plot of genes expressed by astrocytes at FPKM >1, plotted as Log2FC against -log10 p-value comparing BMP6-treated and untreated WT astrocytes. Each dot represents a gene; top right sector genes significantly upregulated (FC>1.5, adjusted p-value <0.05), examples in red; top left sector genes significantly

downregulated (FC<−1.5, adjusted p-value <0.05), examples in turquoise, calculated with DESeq2. **e.** Venn diagram showing overlap between proteins and genes downregulated in WT astrocytes treated with BMP6. For mass spectrometry and RNA Sequencing N=6 cultures, half of each culture treated with BMP6 and other half left untreated. Proteomics, p<0.05, abundance >0.01%, fold change ≥1.5 calculated with Patternlab. RNASeq, adjusted p<0.05, FPKM>1, fold change ≥1.5 calculated with DESeq2.

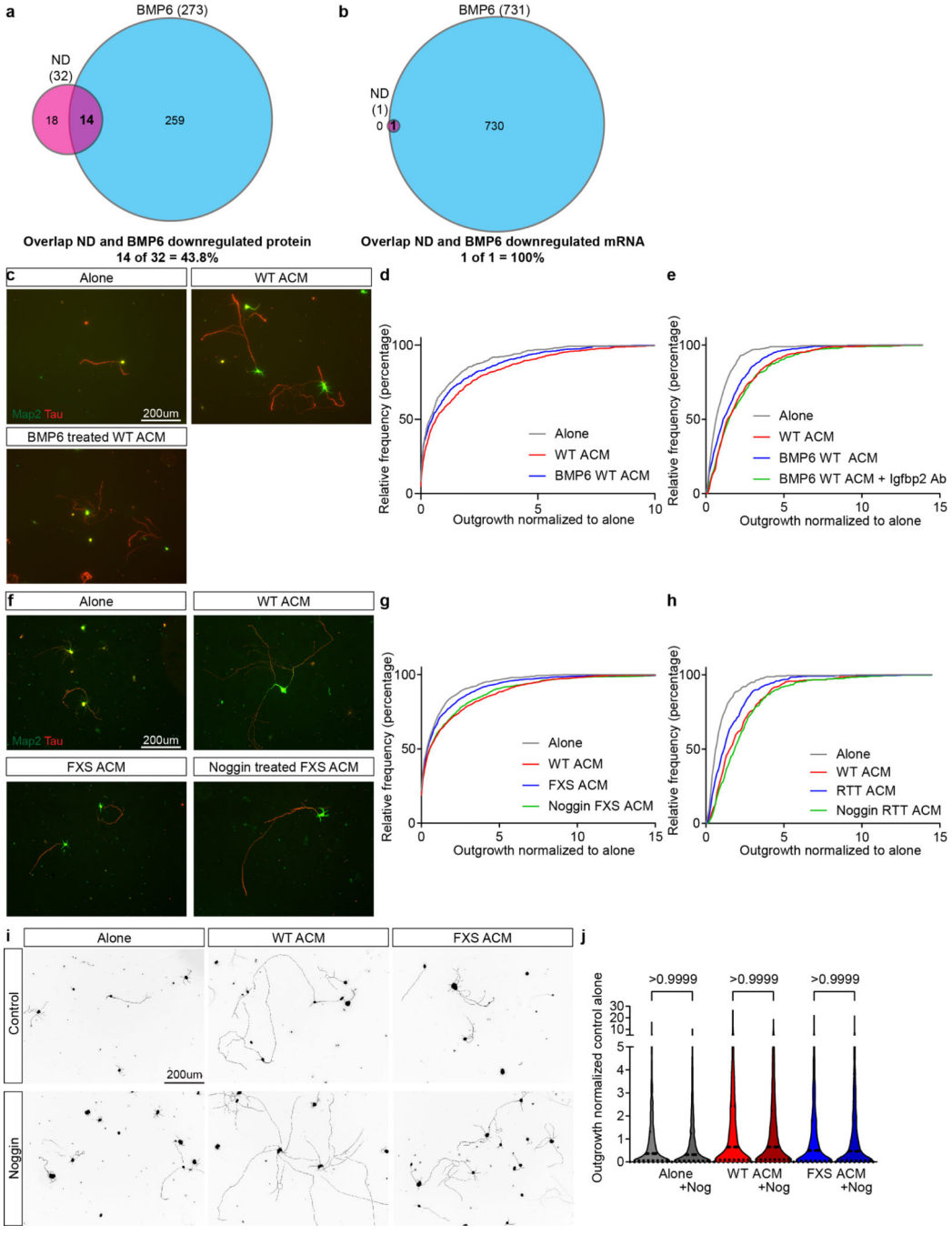

Extended Data Fig. 7. Blocking ND astrocyte BMP signaling reduces neural deficits.

a,b. BMP6-treated WT astrocytes show protein secretion (**a**) and gene expression (**b**) downregulations that overlap with ND astrocytes. N=6 cultures WT, FXS, RTT, DS, plus 6 cultures WT +/− BMP6 proteomics; N=6 cultures WT, FXS, RTT; 4 DS, plus 6 cultures WT +/− BMP6 RNA sequencing. **c.** Example images from Figure 7d prior to processing and analysis. Neurons immunostained with MAP2 (dendrites, green) and tau (axon, red). **d**. Relative frequency distribution plot of total neurite outgrowth length, same data as Figure 7e. Data from 3 experiments, number of neurons: alone=467, WT ACM=733, BMP6 WT ACM=610.**e**. Relative frequency distribution plot of total neurite outgrowth length, same data as Figure 7f. Data from 3 experiments, number of neurons: alone=378, WT ACM=380, BMP6 WT ACM=506, BMP6 WT ACM + Igfbp2 blocking Ab=335. **f.** Example images from Figure 7h prior to processing and analysis. Neurons immunostained with MAP2 (dendrites, green) and tau (axon, red). **g**. Relative frequency distribution plot of total neurite outgrowth, same data as Figure 7i. Data from 3 experiments, number of neurons: alone=923, WT ACM=1164, FXS ACM=1132, Noggin FXS ACM=1099. **h**. Relative frequency distribution plot of total neurite outgrowth, same data as Figure 7j. Data from 3 experiments, number of neurons: alone=238, WT ACM=279, RTT ACM=387, Noggin RTT ACM=365. **i**. Example images of cortical neurons treated with noggin at the time of plating, ± WT ACM or ± FXS ACM (image merge of MAP2 + Tau). **j**. Quantification of total neurite outgrowth, data from 3 experiments. Number of neurons: alone=2197, alone + noggin=1981, WT ACM=2167, WT ACM + noggin=2421, FXS ACM=2060, FXS ACM + noggin=2523. Violin plots dashed line marks median, dotted lines 25th and 75th percentile. Statistics by Kruskal-Wallis one-way ANOVA on ranks with Dunn's test for multiple comparisons.

Supplementary Material

Refer to Web version on PubMed Central for supplementary material.

Acknowledgements

We thank Cari Dowling for technical assistance, and A. Saghatelian, members of the Allen lab and MNL for helpful discussion. This work was supported by a Salk Institute Innovation grant. A.L.M.C. was supported by a Dennis Weatherstone Predoctoral Fellowship from Autism Speaks, and the Chapman Foundation. J.D. is supported by F30 HD106699 from NICHD. N.J.A. is supported by the Chan Zuckerberg Initiative, Hearst Foundation and Pew Foundation. This work was supported by core facilities of the Salk Institute including the Mass Spectrometry Core, Next Generation Sequencing Core, Integrative Genomics and Bioinformatics Core, Waitt Advanced Biophotonics Core, with funding from NIH-NCI CCSG: P30 014195, Chapman Foundation, Waitt Foundation and Helmsley Center for Genomic Medicine. The funders had no role in study design, data collection and analysis, decision to publish or preparation of the manuscript.

References

1. Ebrahimi-Fakhari D.& Sahin M.Autism and the synapse: emerging mechanisms and mechanism-based therapies. Current opinion in neurology 28, 91–102 (2015). [PubMed: 25695134]
2. Amir RE, Van den Veyver IB, Wan M, Tran CQ, Francke U.& Zoghbi HY Rett syndrome is caused by mutations in X-linked MECP2, encoding methyl-CpG-binding protein 2. Nature genetics 23, 185–188 (1999). [PubMed: 10508514]
3. Xu X, Miller EC & Pozzo-Miller L.Dendritic spine dysgenesis in Rett syndrome. Frontiers in Neuroanatomy 8 (2014).
4. Wang ITJ, Reyes A-RS & Zhou Z.Neuronal morphology in MeCP2 mouse models is intrinsically variable and depends on age, cell type, and Mecp2 mutation. Neurobiology of Disease 58, 3–12 (2013). [PubMed: 23659895]

5. Irwin SA, Galvez R.& Greenough WT Dendritic Spine Structural Anomalies in Fragile-X Mental Retardation Syndrome. (2000).
6. Nimchinsky EA, Oberlander AM & Svoboda K.Abnormal development of dendritic spines in FMR1 knock-out mice. J Neurosci 21, 5139–5146 (2001). [PubMed: 11438589]
7. Benavides-Piccione R, Ballesteros-Yanez I, de Lagran MM, Elston G, Estivill X, Fillat C, Defelipe J.& Dierssen M.On dendrites in Down syndrome and DS murine models: a spiny way to learn. Prog Neurobiol 74, 111–126 (2004). [PubMed: 15518956]
8. Blanco-Suárez E, Caldwell ALM & Allen NJ Role of astrocyte–synapse interactions in CNS disorders. The Journal of physiology 595, 1903–1916 (2017). [PubMed: 27381164]
9. Banker G.Trophic interactions between astroglial cells and hippocampal neurons in culture. Science 209, 809–810 (1980). [PubMed: 7403847]
10. Ullian EM, Sapperstein SK, Christopherson KS & Barres BA Control of synapse number by glia. Science 291, 657–661 (2001). [PubMed: 11158678]
11. Araujo BHS, Kaid C, De Souza JS, Gomes da Silva S, Goulart E, Caires LCJ, Musso CM, Torres LB, Ferrasa A, Herai R, Zatz M, Okamoto OK & Cavalheiro EA Down Syndrome iPSC-Derived Astrocytes Impair Neuronal Synaptogenesis and the mTOR Pathway In Vitro. Molecular Neurobiology (2017).
12. Ballas N, Lioy DT, Grunseich C.& Mandel G.Non-cell autonomous influence of MeCP2-deficient glia on neuronal dendritic morphology. Nat Neurosci 12, 311–317 (2009). [PubMed: 19234456]
13. Jacobs S, Nathwani M.& Doering L.Fragile X astrocytes induce developmental delays in dendrite maturation and synaptic protein expression. BMC Neuroscience 11, 132 (2010). [PubMed: 20955577]
14. Meissner F, Scheltema RA, Mollenkopf H-J & Mann M.Direct Proteomic Quantification of the Secretome of Activated Immune Cells. Science 340, 475–478 (2013). [PubMed: 23620052]
15. Johnson ECB, Carter EK, Dammer EB, Duong DM, Gerasimov ES, Liu Y, Liu J, Betarbet R, Ping L, Yin L, Serrano GE, Beach TG, Peng J, De Jager PL, Haroutunian V, Zhang B, Gaiteri C, Bennett DA, Gearing M, Wingo TS, Wingo AP, Lah JJ, Levey AI & Seyfried NT Large-scale deep multi-layer analysis of Alzheimer's disease brain reveals strong proteomic disease-related changes not observed at the RNA level. Nature Neuroscience (2022).
16. Boisvert MM, Erikson GA, Shokhirev MN & Allen NJ The Aging Astrocyte Transcriptome from Multiple Regions of the Mouse Brain. Cell Reports 22, 269–285 (2018). [PubMed: 29298427]
17. Chai H, Diaz-Castro B, Shigetomi E, Monte E, Octeau JC, Yu X, Cohn W, Rajendran PS, Vondriska TM, Whitelegge JP, Coppola G.& Khakh BS Neural Circuit-Specialized Astrocytes: Transcriptomic, Proteomic, Morphological, and Functional Evidence. Neuron 95, 531–549.e539 (2017). [PubMed: 28712653]
18. McCarthy KD & de Vellis J.Preparation of separate astroglial and oligodendroglial cell cultures from rat cerebral tissue. The Journal of Cell Biology 85, 890–902 (1980). [PubMed: 6248568]
19. Foo LC, Allen NJ, Bushong EA, Ventura PB, Chung WS, Zhou L, Cahoy JD, Daneman R, Zong H, Ellisman MH & Barres BA Development of a method for the purification and culture of rodent astrocytes. Neuron 71, 799–811 (2011). [PubMed: 21903074]
20. Foo LC Purification of Rat and Mouse Astrocytes by Immunopanning. Cold Spring Harbor Protocols 2013, pdb.prot074211 (2013).
21. Batiuk MY, de Vin F, Duqué SI, Li C, Saito T, Saido T, Fiers M, Belgard TG & Holt MG An immunoaffinity-based method for isolating ultrapure adult astrocytes based on ATP1B2 targeting by the ACSA-2 antibody. Journal of Biological Chemistry 292, 8874–8891 (2017). [PubMed: 28373281]
22. Kantzer C, Boutin C, Herzig ID, Wittwer C, Reiß S, Tiveron MC, Drewes J, Rockel TD, Ohlig S, Ninkovic J, Cremer H, Pennartz S, Jungblut M.& Bosio A.Anti-ACSA-2 defines a novel monoclonal antibody for prospective isolation of living neonatal and adult astrocytes. Glia 65, 990–1004 (2017). [PubMed: 28317180]
23. Steinmetz CC, Buard I, Claudepierre T, Nägler K.& Pfrieger FW Regional variations in the glial influence on synapse development in the mouse CNS. The Journal of physiology 577, 249–261 (2006). [PubMed: 16959855]

24. Williams EC, Zhong X, Mohamed A, Li R, Liu Y, Dong Q, Ananiev GE, Mok JCC, Lin BR, Lu J, Chiao C, Cherney R, Li H, Zhang S-C & Chang Q.Mutant astrocytes differentiated from Rett syndrome patients-specific iPSCs have adverse effects on wild-type neurons. Human Molecular Genetics 23, 2968–2980 (2014). [PubMed: 24419315]
25. Allen NJ & Eroglu C.Cell Biology of Astrocyte-Synapse Interactions. Neuron 96, 697–708 (2017). [PubMed: 29096081]
26. Yang YH, Nam MS & Yang ES Rapid prenatal diagnosis of trisomy 21 by real-time quantitative polymerase chain reaction with amplification of small tandem repeats and S100B in chromosome 21. Yonsei Med J 46, 193–197 (2005). [PubMed: 15861490]
27. Higashimori H, Schin CS, Chiang MSR, Morel L, Shoneye TA, Nelson DL & Yang Y.Selective Deletion of Astroglial FMRP Dysregulates Glutamate Transporter GLT1 and Contributes to Fragile X Syndrome Phenotypes In Vivo. The Journal of Neuroscience 36, 7079–7094 (2016). [PubMed: 27383586]
28. Higashimori H, Morel L, Huth J, Lindemann L, Dulla C, Taylor A, Freeman M.& Yang Y.Astroglial FMRP-dependent translational down-regulation of mGluR5 underlies glutamate transporter GLT1 dysregulation in the fragile X mouse. Human Molecular Genetics 22, 2041–2054 (2013). [PubMed: 23396537]
29. Yuskaitis CJ, Beurel E.& Jope RS Evidence of reactive astrocytes but not peripheral immune system activation in a mouse model of Fragile X syndrome. Biochimica et Biophysica Acta (BBA) - Molecular Basis of Disease 1802, 1006–1012 (2010). [PubMed: 20600866]
30. Liddelow SA, Guttenplan KA, Clarke LE, Bennett FC, Bohlen CJ, Schirmer L, Bennett ML, Münch AE, Chung W-S, Peterson TC, Wilton DK, Frouin A, Napier BA, Panicker N, Kumar M, Buckwalter MS, Rowitch DH, Dawson VL, Dawson TM, Stevens B.& Barres BA Neurotoxic reactive astrocytes are induced by activated microglia. Nature 541, 481 (2017). [PubMed: 28099414]
31. Blanco-Suarez E, Liu T-F, Kopelevich A.& Allen NJ Astrocyte-Secreted Chordin-like 1 Drives Synapse Maturation and Limits Plasticity by Increasing Synaptic GluA2 AMPA Receptors. Neuron 100, 1116–1132.e1113 (2018). [PubMed: 30344043]
32. Molofsky AV, Kelley KW, Tsai H-H, Redmond SA, Chang SM, Madireddy L, Chan JR, Baranzini SE, Ullian EM & Rowitch DH Astrocyte-encoded positional cues maintain sensorimotor circuit integrity. Nature 509, 189–194 (2014). [PubMed: 24776795]
33. Scholze AR, Foo LC, Mulinyawe S.& Barres BA BMP Signaling in Astrocytes Downregulates EGFR to Modulate Survival and Maturation. PloS one 9, e110668 (2014).
34. Yang Q, Feng B, Zhang K, Guo Y. y., Liu S. b., Wu Y. m., Li X. q. & Zhao M-g. Excessive Astrocyte-Derived Neurotrophin-3 Contributes to the Abnormal Neuronal Dendritic Development in a Mouse Model of Fragile X Syndrome. PLoS Genet 8, e1003172 (2012).
35. Vilardell M, Rasche A, Thormann A, Maschke-Dutz E, Pérez-Jurado LA, Lehrach H.& Herwig R.Meta-analysis of heterogeneous Down Syndrome data reveals consistent genome-wide dosage effects related to neurological processes. BMC Genomics 12, 229 (2011). [PubMed: 21569303]
36. Ballestín R, Blasco-Ibáñez JM, Crespo C, Nacher J, López-Hidalgo R, Gilabert-Juan J, Moltó D.& Varea E.Astrocytes of the murine model for Down Syndrome Ts65Dn display reduced intracellular ionic zinc. Neurochemistry International 75, 48–53 (2014). [PubMed: 24911951]
37. Costales J.& Kolevzon A.The therapeutic potential of insulin-like growth factor-1 in central nervous system disorders. Neuroscience & Biobehavioral Reviews 63, 207–222 (2016). [PubMed: 26780584]
38. Woronowicz A, Cawley NX, Chang S-Y, Koshimizu H, Phillips AW, Xiong Z-G & Loh YP Carboxypeptidase E knockout mice exhibit abnormal dendritic arborization and spine morphology in central nervous system neurons. Journal of Neuroscience Research 88, 64–72 (2010). [PubMed: 19598241]
39. Zhang Y, Chen K, Sloan SA, Bennett ML, Scholze AR, O'Keeffe S, Phatnani HP, Guarnieri P, Caneda C, Ruderisch N, Deng S, Liddelow SA, Zhang C, Daneman R, Maniatis T, Barres BA & Wu JQ An RNA-Sequencing Transcriptome and Splicing Database of Glia, Neurons, and Vascular Cells of the Cerebral Cortex. The Journal of Neuroscience 34, 11929–11947 (2014). [PubMed: 25186741]

40. Chen C, Jiang P, Xue H, Peterson SE, Tran HT, McCann AE, Parast MM, Li S, Pleasure DE, Laurent LC, Loring JF, Liu Y.& Deng W.Role of astroglia in Down's syndrome revealed by patient-derived human-induced pluripotent stem cells. Nat Com 5 (2014).
41. Marchetto MCN, Carromeu C, Acab A, Yu D, Yeo GW, Mu Y, Chen G, Gage FH & Muotri AR A Model for Neural Development and Treatment of Rett Syndrome Using Human Induced Pluripotent Stem Cells. Cell 143, 527–539 (2010). [PubMed: 21074045]
42. Wang RN, Green J, Wang Z, Deng Y, Qiao M, Peabody M, Zhang Q, Ye J, Yan Z, Denduluri S, Idowu O, Li M, Shen C, Hu A, Haydon RC, Kang R, Mok J, Lee MJ, Luu HL & Shi LL Bone Morphogenetic Protein (BMP) signaling in development and human diseases. Genes & Diseases 1, 87–105 (2014). [PubMed: 25401122]
43. Verkhratsky A, Matteoli M, Parpura V, Mothet J-P & Zorec R.Astrocytes as secretory cells of the central nervous system: idiosyncrasies of vesicular secretion. The EMBO journal 35, 239–257 (2016). [PubMed: 26758544]
44. Branon TC, Bosch JA, Sanchez AD, Udeshi ND, Svinkina T, Carr SA, Feldman JL, Perrimon N.& Ting AY Efficient proximity labeling in living cells and organisms with TurboID. Nature Biotechnology 36, 880 (2018).
45. Bayraktar OA, Bartels T, Holmqvist S, Kleshchevnikov V, Martirosyan A, Polioudakis D, Ben Haim L, Young AMH, Batiuk MY, Prakash K, Brown A, Roberts K, Paredes MF, Kawaguchi R, Stockley JH, Sabeur K, Chang SM, Huang E, Hutchinson P, Ullian EM, Hemberg M, Coppola G, Holt MG, Geschwind DH & Rowitch DH Astrocyte layers in the mammalian cerebral cortex revealed by a single-cell in situ transcriptomic map. Nature Neuroscience 23, 500–509 (2020). [PubMed: 32203496]
46. Kashima R, Roy S, Ascano M, Martinez-Cerdeno V, Ariza-Torres J, Kim S, Louie J, Lu Y, Leyton P, Bloch KD, Kornberg TB, Hagerman PJ, Hagerman R, Lagna G.& Hata A.Augmented noncanonical BMP type II receptor signaling mediates the synaptic abnormality of fragile X syndrome. Science Signaling 9, ra58-ra58 (2016).
47. Chen J, Alberts I.& Li X.Dysregulation of the IGF-I/PI3K/AKT/mTOR signaling pathway in autism spectrum disorders. International Journal of Developmental Neuroscience 35, 35–41 (2014). [PubMed: 24662006]
48. Izumi K, Kellogg E, Fujiki K, Kaur M, Tilton RK, Noon S, Wilkens A, Shirahige K.& Krantz ID Elevation of insulin-like growth factor binding protein-2 level in Pallister–Killian syndrome: Implications for the postnatal growth retardation phenotype. American Journal of Medical Genetics Part A 167, 1268–1274 (2015). [PubMed: 25900123]
49. Itoh M, Ide S, Takashima S, Kudo S, Nomura Y, Segawa M, Kubota T, Mori H, Tanaka S, Horie H, Tanabe Y.& Goto Y.-i Methyl CpG-Binding Protein 2 (a Mutation of Which Causes Rett Syndrome) Directly Regulates Insulin-Like Growth Factor Binding Protein 3 in Mouse and Human Brains. *Journal of Neuropathology &* Experimental Neurology 66, 117–123 (2007).
50. Degano AL, Pasterkamp RJ & Ronnett GV MeCP2 deficiency disrupts axonal guidance, fasciculation, and targeting by altering Semaphorin 3F function. Molecular and cellular neurosciences 42, 243–254 (2009). [PubMed: 19628041]
51. Menon L.& Mihailescu M-R Interactions of the G quartet forming semaphorin 3F RNA with the RGG box domain of the fragile X protein family. Nucleic Acids Research 35, 5379–5392 (2007). [PubMed: 17693432]
52. Abouzied MM, El-Tahir HM, Gieselmann V.& Franken S.Hepatoma-derived growth factor-related protein-3: A new neurotrophic and neurite outgrowth-promoting factor for cortical neurons. Journal of Neuroscience Research 88, 3610–3620 (2010). [PubMed: 20890995]
53. Kalus I, Rohn S, Puvirajesinghe TM, Guimond SE, Eyckerman-Kölln PJ, Ten Dam G, van Kuppevelt TH, Turnbull JE & Dierks T.Sulf1 and Sulf2 Differentially Modulate Heparan Sulfate Proteoglycan Sulfation during Postnatal Cerebellum Development: Evidence for Neuroprotective and Neurite Outgrowth Promoting Functions. PloS one 10, e0139853-e0139853 (2015).
54. Bao X, Mikami T, Yamada S, Faissner A, Muramatsu T.& Sugahara K.Heparin-binding Growth Factor, Pleiotrophin, Mediates Neuritogenic Activity of Embryonic Pig Brain-derived Chondroitin Sulfate/Dermatan Sulfate Hybrid Chains. Journal of Biological Chemistry 280, 9180–9191 (2005). [PubMed: 15632143]

55. Krencik R, Hokanson KC, Narayan AR, Dvornik J, Rooney GE, Rauen KA, Weiss LA, Rowitch DH & Ullian EM Dysregulation of astrocyte extracellular signaling in Costello syndrome. Science Translational Medicine 7, 286ra266–286ra266 (2015).

56. Malter JS, Ray BC, Westmark PR & Westmark CJ Fragile X Syndrome and Alzheimer's Disease: Another story about APP and beta-amyloid. Curr Alzheimer Res 7, 200–206 (2010). [PubMed: 20088809]

57. Seritan AL, Nguyen DV, Farias ST, Hinton L, Grigsby J, Bourgeois JA & Hagerman RJ Dementia in fragile X-associated tremor/ataxia syndrome (FXTAS): comparison with Alzheimer's disease. Am J Med Genet B Neuropsychiatr Genet 147B, 1138–1144 (2008). [PubMed: 18384046]

58. Bonham LW, Geier EG, Steele NZR, Holland D, Miller BL, Dale AM, Desikan RS, Yokoyama JS & , A. s. DNI Insulin-Like Growth Factor Binding Protein 2 Is Associated With Biomarkers of Alzheimer's Disease Pathology and Shows Differential Expression in Transgenic Mice. Frontiers in Neuroscience 12 (2018).

Methods References

59. Guy J, Hendrich B, Holmes M, Martin JE & Bird A.A mouse Mecp2-null mutation causes neurological symptoms that mimic Rett syndrome. Nature genetics 27, 322–326 (2001). [PubMed: 11242117]

60. Bakker CE, Verheij C, Willemsen R, van der Helm R, Oerlemans F, Vermey M, Bygrave A, Hoogeveen A, Oostra BA, Reyniers E, De Boule K, D'Hooge R, Cras P, van Velzen D, Nagels G, Martin J-J, De Deyn PP, Darby JK & Willems PJ Fmr1 knockout mice: A model to study fragile X mental retardation. Cell 78, 23–33 (1994). [PubMed: 8033209]

61. Gupta M, Dhanasekaran AR & Gardiner KJ Mouse models of Down syndrome: gene content and consequences. Mamm Genome 27, 538–555 (2016). [PubMed: 27538963]

62. Davisson MT, Schmidt C.& Akeson EC Segmental trisomy of murine chromosome 16: a new model system for studying Down syndrome. Progress in clinical and biological research 360, 263–280 (1990). [PubMed: 2147289]

63. Duchon A, Raveau M, Chevalier C, Nalesso V, Sharp AJ & Herault Y.Identification of the translocation breakpoints in the Ts65Dn and Ts1Cje mouse lines: relevance for modeling Down syndrome. Mamm Genome 22, 674–684 (2011). [PubMed: 21953411]

64. Kahlem P, Sultan M, Herwig R, Steinfath M, Balzereit D, Eppens B, Saran NG, Pletcher MT, South ST, Stetten G, Lehrach H, Reeves RH & Yaspo M-L Transcript Level Alterations Reflect Gene Dosage Effects Across Multiple Tissues in a Mouse Model of Down Syndrome. Genome Research 14, 1258–1267 (2004). [PubMed: 15231742]

65. Yu T, Li Z, Jia Z, Clapcote SJ, Liu C, Li S, Asrar S, Pao A, Chen R, Fan N, Carattini-Rivera S, Bechard AR, Spring S, Henkelman RM, Stoica G, Matsui S-I, Nowak NJ, Roder JC, Chen C, Bradley A.& Yu YE A mouse model of Down syndrome trisomic for all human chromosome 21 syntenic regions. Human Molecular Genetics 19, 2780–2791 (2010). [PubMed: 20442137]

66. Bansal R.& Pfeiffer SE Reversible inhibition of oligodendrocyte progenitor differentiation by a monoclonal antibody against surface galactolipids. Proceedings of the National Academy of Sciences 86, 6181–6185 (1989).

67. Farhy-Tselnicker I, van Casteren ACM, Lee A, Chang VT, Aricescu AR & Allen NJ Astrocyte-Secreted Glypican 4 Regulates Release of Neuronal Pentraxin 1 from Axons to Induce Functional Synapse Formation. Neuron 96, 428–445.e413 (2017). [PubMed: 29024665]

68. Winzeler A.& Wang JT Purification and culture of retinal ganglion cells from rodents. Cold Spring Harb Protoc 2013, 643–652 (2013). [PubMed: 23818667]

69. Xu T, Park SK, Venable JD, Wohlschlegel JA, Diedrich JK, Cociorva D, Lu B, Liao L, Hewel J, Han X, Wong CCL, Fonslow B, Delahunty C, Gao Y, Shah H.& Yates JR 3rd. ProLuCID: An improved SEQUEST-like algorithm with enhanced sensitivity and specificity. J Proteomics 129, 16–24 (2015). [PubMed: 26171723]

70. Carvalho PC, Lima DB, Leprevost FV, Santos MDM, Fischer JSG, Aquino PF, Moresco JJ, Yates JR 3rd & Barbosa VC Integrated analysis of shotgun proteomic data with PatternLab for proteomics 4.0. Nature protocols 11, 102–117 (2016). [PubMed: 26658470]

71. Zybailov B, Mosley AL, Sardiu ME, Coleman MK, Florens L.& Washburn MP Statistical Analysis of Membrane Proteome Expression Changes in Saccharomyces cerevisiae. Journal of Proteome Research 5, 2339–2347 (2006). [PubMed: 16944946]

72. Mi H, Huang X, Muruganujan A, Tang H, Mills C, Kang D.& Thomas PD PANTHER version 11: expanded annotation data from Gene Ontology and Reactome pathways, and data analysis tool enhancements. Nucleic Acids Research 45, D183–D189 (2017). [PubMed: 27899595]

73. Farhy-Tselnicker I, Boisvert MM, Liu H, Dowling C, Erikson GA, Blanco-Suarez E, Farhy C, Shokhirev MN, Ecker JR & Allen NJ Activity-dependent modulation of synapse-regulating genes in astrocytes. eLife 10, e70514 (2021).

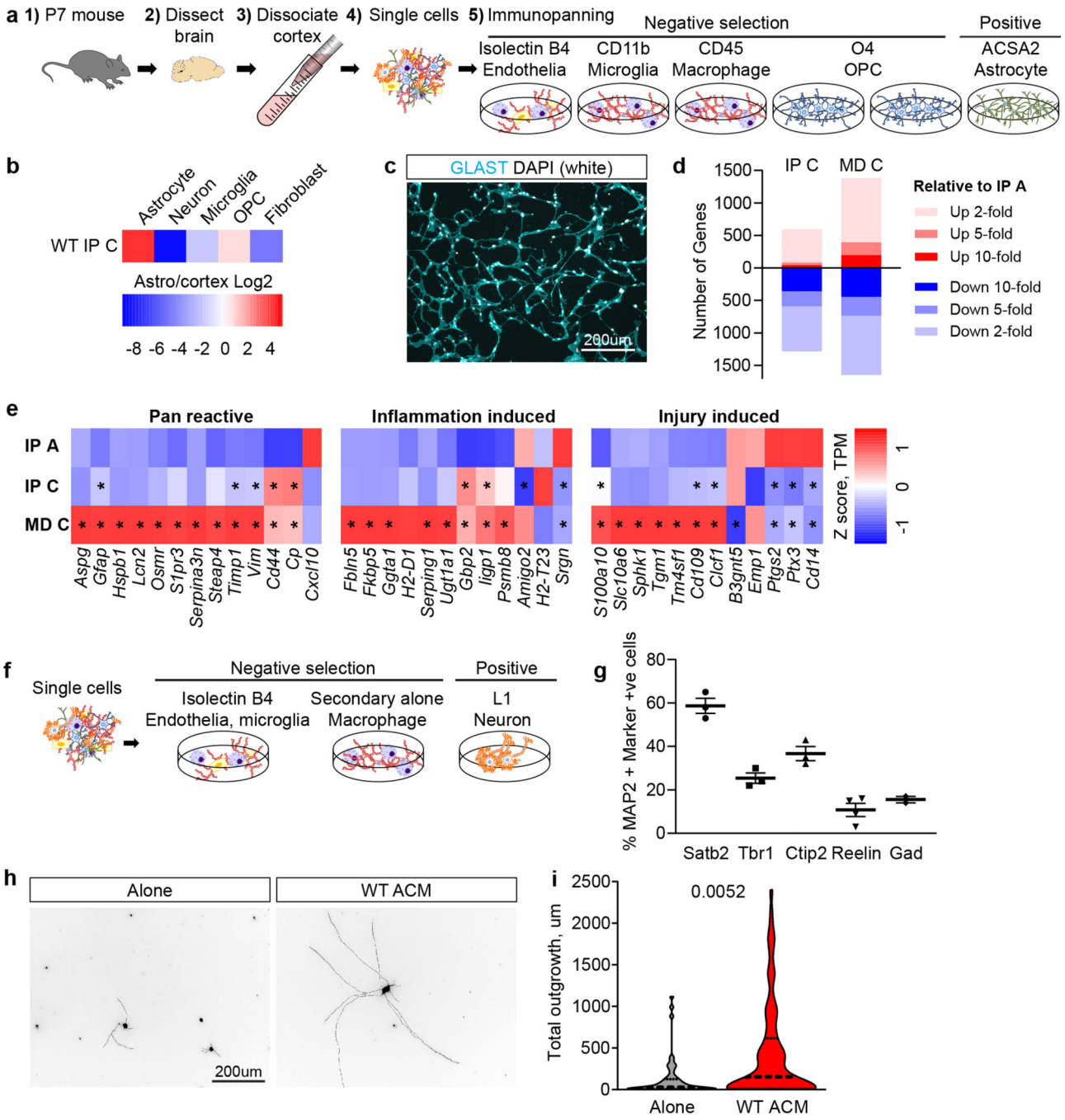

Figure 1. Immunopanned astrocyte and neuron cultures for study of NDs.

a. Schematic: P7 mouse cortex is digested with papain producing a single cell suspension, followed by negative selection to deplete unwanted cells (endothelia, microglia, oligodendrocyte precursor cells (OPCs)), and positive selection for astrocytes using an antibody against ACSA2. **b.** qRT-PCR for cell-type markers from IP astrocyte mRNA compared to P7cortex demonstrates enrichment for astrocytes (Gfap), and depletion of neurons (Syt1), microglia (Cd68), fibroblasts (Fgfr4), OPCs (Cspg4) in WT astrocyte cultures. N=6 cultures. **c.** Immunostaining IP-astrocyte cultures for astrocyte marker GLAST

(cyan, Slc1a3) and nuclei (white, DAPI) demonstrates majority of cells express this protein, repeated 3 separate cultures. **d-e.** Comparison of cultured immunopanned astrocyte (IP C) gene expression to acutely isolated immunopanned astrocytes (IP A) and traditional astrocyte cultures (MD C) using RNA sequencing. **d.** Number of differentially expressed genes between IP A and IP C or MD C. N=3 cultures/condition; adjusted $p<0.05$, TPM>10, calculated with DESeq2. **e.** Relative expression of reactive astrocyte genes between IP A, IP C and MD C astrocytes, plotted as z-score of TPM. *adjusted $p<0.05$ compared to IP A calculated with DESeq2. **f-i.** WT ACM supports WT neurite outgrowth. **f.** Schematic of immunopanning procedure to isolate cortical neurons: P7 mouse cortex is digested with papain producing a single cell suspension, followed by negative selection to deplete unwanted cells (endothelia, microglia), and positive selection for neurons using an antibody against NCAM-L1. **g.** Characterization of cortical neuron subtypes in immunopanned cultures, percentage of MAP2 positive cells expressing the cortical neuron subtype marker. Graph mean±s.e.m., individual data points average of experiment. N=3 experiments SATB2, TBR1, CTIP2; N=4 Reelin; N=2 GAD. **h-i.** Culturing WT cortical neurons for 48 hours with WT astrocyte conditioned media (ACM) increases neurite outgrowth. **h.** Example images, neurons immunostained with MAP2 and tau, merged image shown. **i.** Quantification of total neurite outgrowth (dendrite + axon; MAP2 + tau). Example experiment shown, repeated 3 times with same result. Number of neurons: alone=51, WT ACM=75. Violin plot: dashed line median, dotted lines 25^{th} and 75^{th} percentile. Statistics by 2-sided Mann-Whitney test. See also Extended Data Figure 1; Table S1.

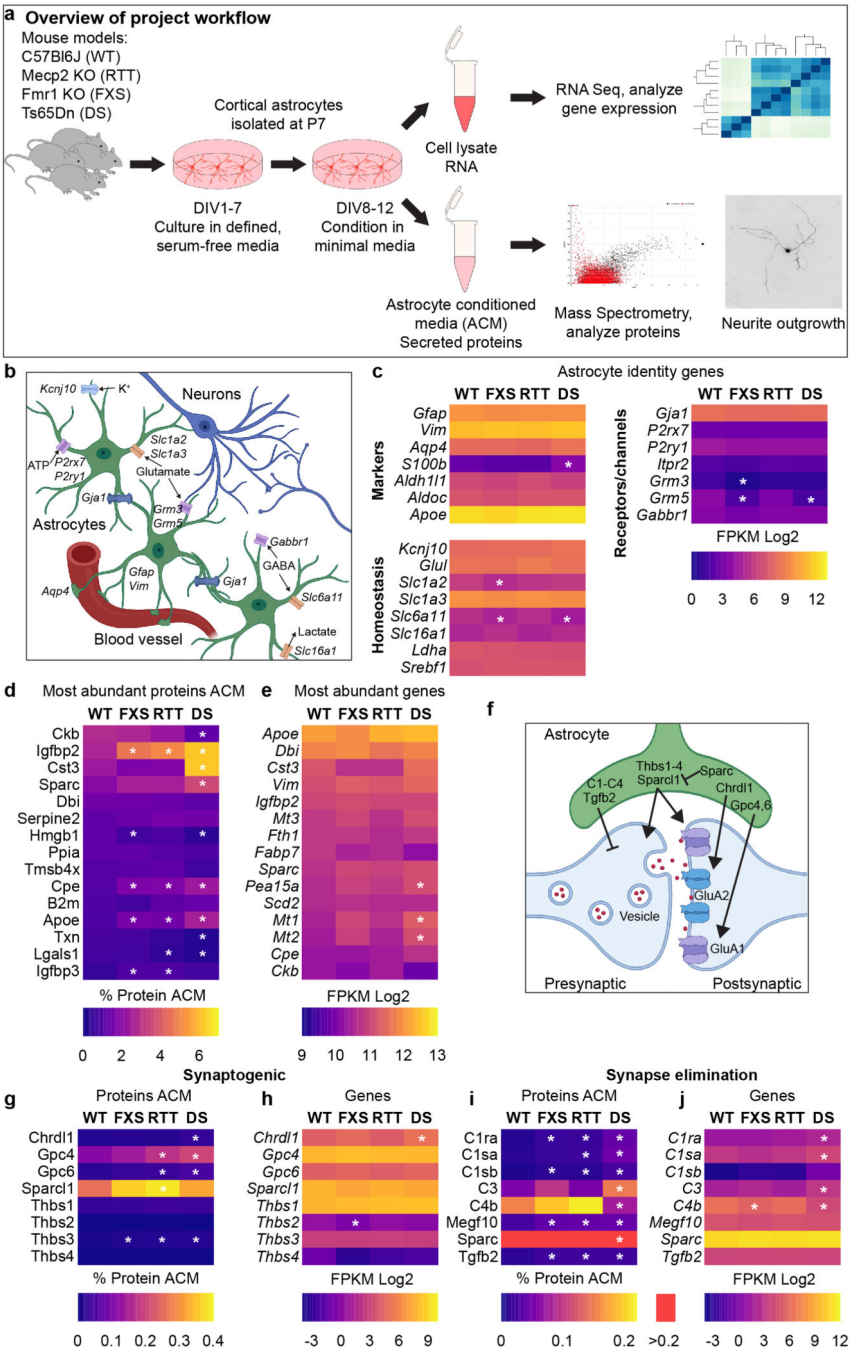

Figure 2. IP astrocytes reproduce in vivo alterations to ND astrocytes.

a. Overview of project workflow. **b,c.** WT and ND IP astrocytes express many known astrocyte markers at high levels. **b.** Astrocytes (green) express cell-specific markers that determine their cellular identity; contact blood vessels and neuronal synapses to engage in metabolism and homeostatic functions; bind and respond to neurotransmitters released by neurons. **c.** Heatmap shows few differences between ND and WT expression of astrocyte identity and function markers. **d.** Heatmap of most abundant proteins, ranked by level in WT ACM. **e.** Heatmap of most abundant mRNA, ranked by level in WT astrocytes. **f-j.**

Schematic of the tripartite synapse (**f**) displaying astrocyte-secreted proteins important for regulating synapse formation and function. **g-j.** Heatmaps of secreted synaptogenic proteins in ACM (**g**) and expression of synaptogenic genes (**h**), as well as abundance of synapse eliminating proteins in ACM (**i**) and corresponding expression of synapse elimination genes (**j**). For the heatmaps a darker shade of red indicates a value above the top of the scale. Proteomics, N=6 cultures per genotype, *$p<0.05$, abundance >0.01%, fold change between WT and ND ≥1.5 calculated with T-fold test in Patternlab. RNASeq, N=6 cultures WT, RTT, FXS; 4 cultures DS, *adjusted $p<0.05$, FPKM>1, fold change between ND and WT ≥1.5 calculated with DESeq2. See also Extended Data Figure 2; Tables S2, S3, S4.

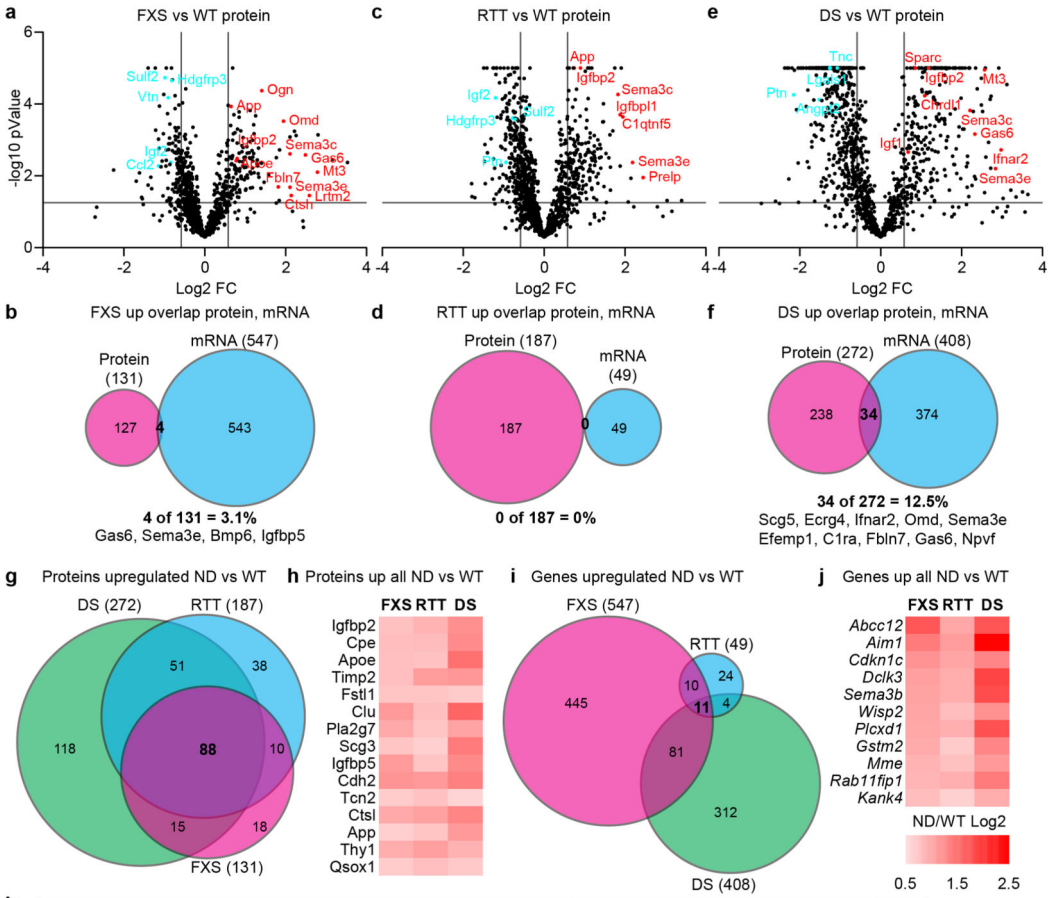

k

PROTEIN UP - PANTHER Pathways	FXS (FDR)	RTT (FDR)	DS (FDR)	ND (FDR)
Alzheimer disease-amyloid secretase pathway (P00003)	1.11E-05	1.41E-04	2.43E-03	4.39E-07
Integrin signalling pathway (P00034)	n/a	3.54E-03	6.26E-02	n/a
Blood coagulation (P00011)	1.04E-02	n/a	n/a	n/a
CCKR signaling map (P06959)	n/a	n/a	4.38E-02	n/a

PROTEIN UP - Reactome pathways	FXS (FDR)	RTT (FDR)	DS (FDR)	ND (FDR)
Post-translational protein phosphorylation (R-MMU-8957275)	1.18E-07	2.16E-17	8.37E-17	1.72E-06
Regulation of IGF transport and uptake by IGFBPs (R-MMU-381426)	1.60E-08	5.31E-17	9.27E-18	1.43E-06
Glycosaminoglycan metabolism (R-MMU-1630316)	1.18E-05	7.59E-11	1.15E-14	9.96E-05
Regulation of Complement cascade (R-MMU-977606)	n/a	3.56E-02	2.81E-02	4.29E-02
Plasma lipoprotein remodeling (R-MMU-8963899)	3.86E-02	4.74E-02	n/a	n/a
Peptide hormone metabolism (R-MMU-2980736)	n/a	n/a	1.01E-02	n/a
Degradation of the extracellular matrix (R-MMU-1474228)	2.50E-03	3.47E-05	2.00E-05	n/a
Axon guidance (R-MMU-422475)	n/a	n/a	2.07E-03	n/a

PROTEIN UP - PANTHER Protein Class	FXS (FDR)	RTT (FDR)	DS (FDR)	ND (FDR)
extracellular matrix protein (PC00102)	4.48E-03	1.77E-04	1.20E-05	1.96E-02
serine protease inhibitor (PC00204)	3.90E-03	2.98E-03	8.84E-04	3.58E-02
complement component (PC00078)	4.20E-02	n/a	n/a	n/a

Figure 3. Altered protein secretion and gene levels of ND astrocytes.

a,c,e. Volcano plot of proteins present in ACM at >0.01%, plotted as Log2FC against -log10 p-value comparing each disorder to WT: FXS (**a**), RTT (**c**) and DS (**e**). Each dot represents a protein; top right sector proteins significantly upregulated (FC>1.5, p-value <0.05), examples in red; top left sector proteins significantly downregulated (FC<−1.5, p-value <0.05), examples in turquoise; calculated with T-fold test in Patternlab. **b,d,f.** Venn diagram of overlap between proteins and genes with increased level in FXS (**b**), RTT (**d**) and DS (**f**) ACM and astrocytes. **g,h.** Venn diagram showing overlap in proteins upregulated in all

NDs (**g**), and heatmap of top altered proteins ranked by protein abundance in FXS ACM (**h**). **i,j.** Venn diagram showing number of genes upregulated in all NDs (**i**) and corresponding heatmap (**j**) of altered genes. Scale bar in **j** also applies to heatmap in **h**. **k.** Pathway analysis of proteins upregulated in ND ACM compared to WT demonstrates overlapping alterations in ND astrocyte function compared to WT, performed using PANTHER over-representation test with Fisher's Exact test and FDR corrected. Proteomics, N=6 cultures per genotype, $p<0.05$, abundance >0.01%, fold change between WT and ND ≥1.5 calculated with T-fold test in Patternlab. RNASeq, N=6 cultures WT, RTT, FXS; 4 cultures DS, adjusted $p<0.05$, FPKM>1, fold change between ND and WT ≥1.5 calculated with DESeq2. See also Extended Data Figure 3; Tables S5, S6, S7, S8, S9.

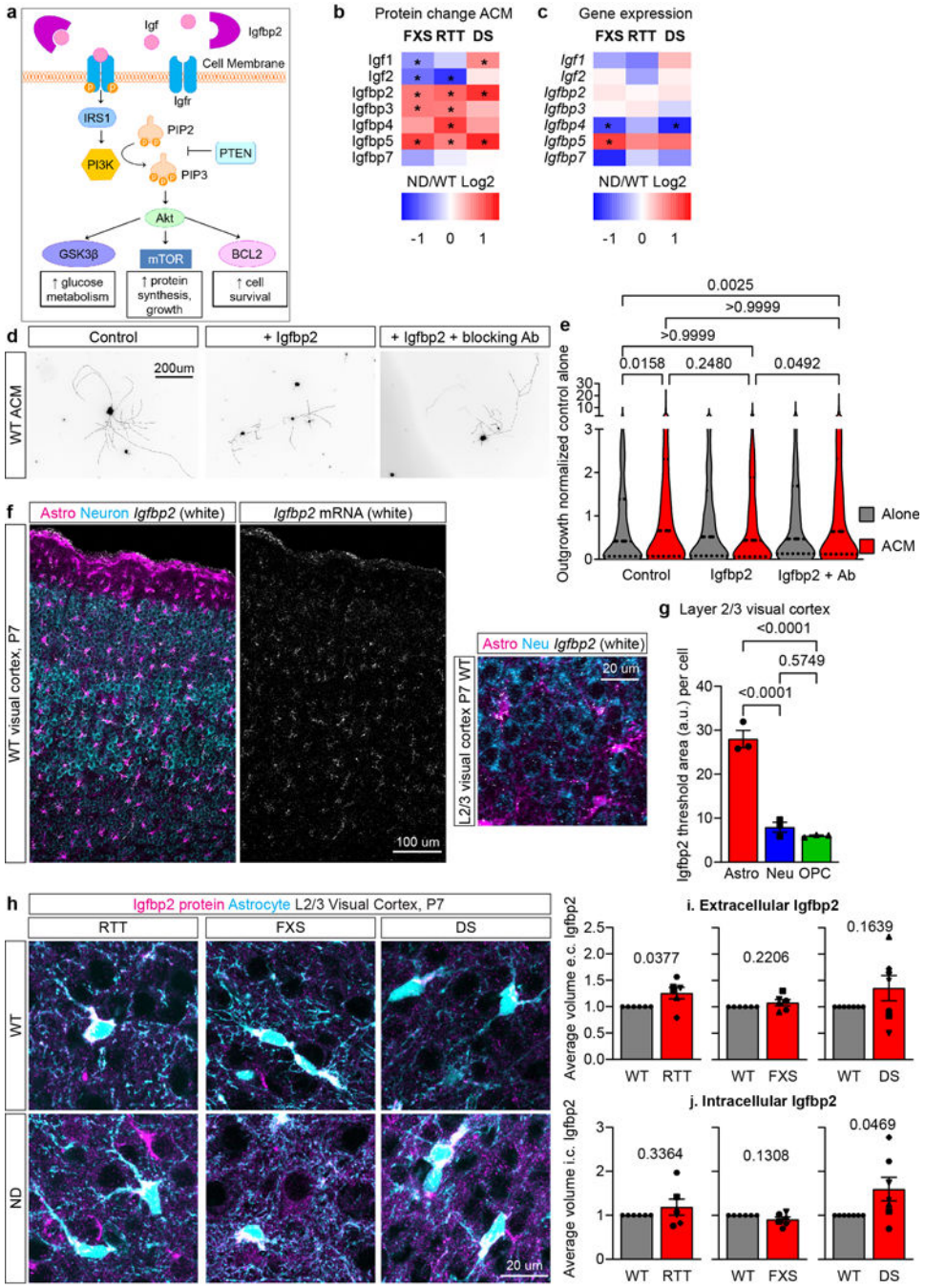

Figure 4. Excess Igfbp2 in ACM inhibits neurite outgrowth.

a. Schematic of IGF signaling via the PI3K/Akt pathway. **b,c.** Protein secretion (**b**) and gene expression (**c**) profiles of IGF family members in WT and ND astrocytes. Proteomics, N=6 cultures/genotype, *p<0.05, abundance >0.01%, fold change between WT and ND ≥1.5 calculated with T-fold test in Patternlab. RNASeq, N=6 cultures WT, RTT, FXS; 4 cultures DS, *adjusted p<0.05, FPKM>1, fold change between ND and WT ≥1.5 calculated with DESeq2. **d,e.** Excess Igfbp2 in ACM inhibits WT neurite outgrowth. **d.** Example images WT neurons grown 48 hours, conditions as marked (image merge of MAP2 + Tau). **e.**

Quantification total neurite outgrowth normalized to control alone condition. Violin plot: dashed line median, dotted lines 25th and 75th percentile. Data from 3 separate experiments, number of neurons: control alone=447, control ACM=626, Igfbp2 alone=438, Igfbp2 ACM=596, Igfbp2 + Ab alone=376, Igfbp2 + Ab + ACM=562. Statistics by Kruskal-Wallis one-way ANOVA on ranks with Dunn's test for multiple comparisons. **f, g.** Astrocytes express Igfbp2 mRNA in the P7 mouse visual cortex. **f.** smFISH against Igfbp2 mRNA in Aldh1l1-GFP mice to mark astrocytes, combined with probe for neurons (Tubb3). Left panels overview of cortex across all layers, right panel high power image from L2/3. **g.** Analysis of images in **f**, expression of Igfbp2 mRNA within astrocytes, neurons and OPCs. See Figure S4d for OPC image. N=3 WT mice. Bar graph mean±s.e.m., individual data points mice; statistics by one-way ANOVA with Tukey's test for multiple comparisons. **h-j.** Immunostaining for Igfbp2 in each ND and littermate WT visual cortex at P7 (RTT - Mecp2 KO; FXS – Fmr1 KO; DS - Ts65Dn TG) reveals an increase in extracellular Igfbp2 in RTT and intracellular Igfbp2 in DS. **h.** Example images of L2/3 astrocytes (cyan, Aldh1l1-GFP) immunostained for Igfbp2 (magenta). **i.** Quantification of extracellular Igfbp2. **j.** Quantification of intracellular Igfbp2. N=6 littermate pairs RTT and FXS; 7 littermate pairs DS. Bar graph mean±s.e.m., individual points mice, same mouse in i and j for each genotype denoted with same shape; statistics two-sided T-test. See also Extended Data Figure 4.

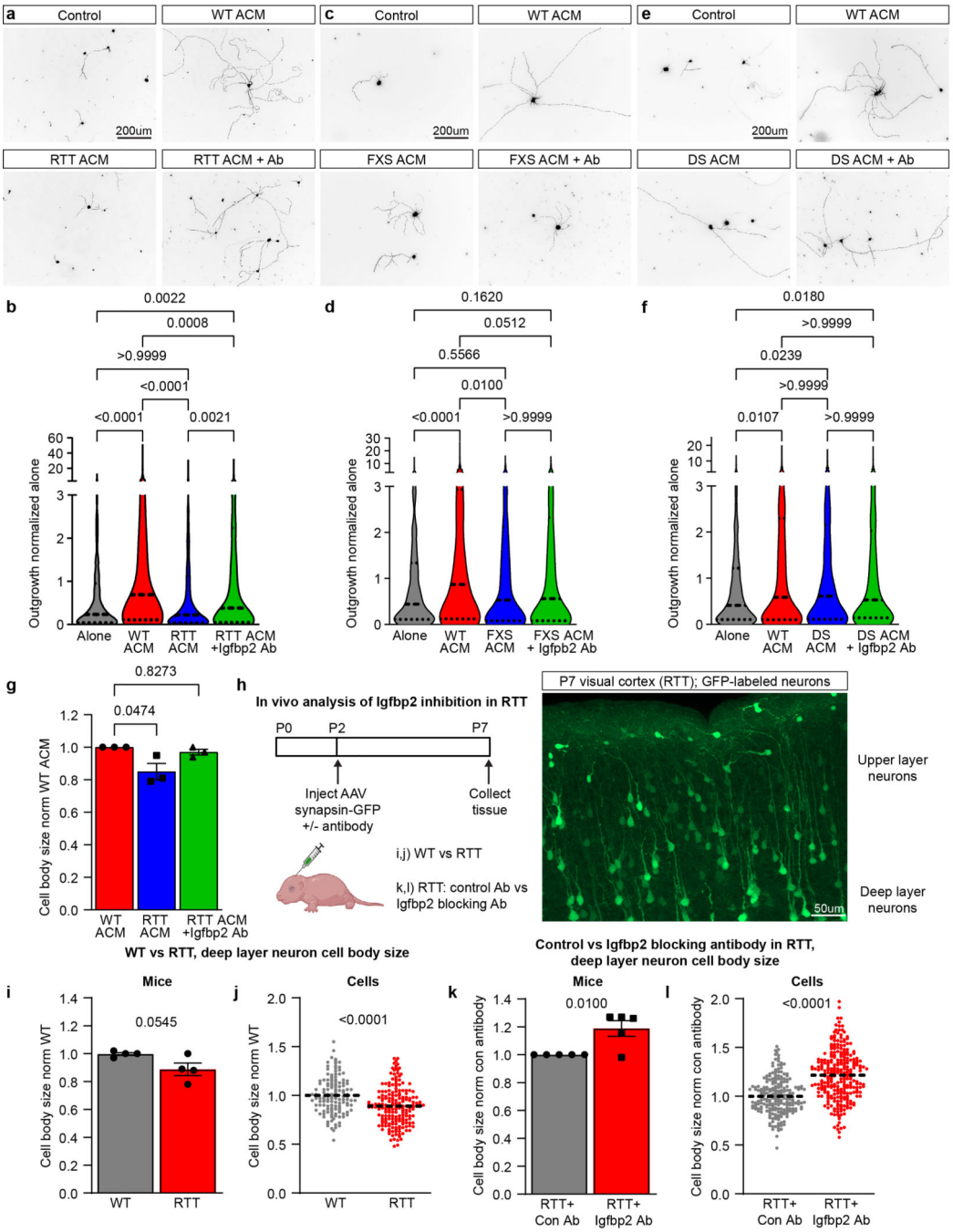

Figure 5. Blocking Igfbp2 in RTT reduces neural developmental deficits.

a-f. Application of an Igfbp2-neutralizing antibody reduces WT neurite outgrowth inhibition induced by RTT ACM. **a,c,e.** Example images neurons cultured for 48 hours in RTT (**a**), FXS (**c**) or DS (**e**) ACM (merged images of MAP2 + Tau). **b,d,f.** Quantification total neurite outgrowth, normalized to alone condition. Violin plot: dashed line median, dotted lines 25th and 75th percentile. Data from 3 (**b**), 4 (**d**), 5 (**f**) separate experiments. Number of neurons: RTT (**b**): alone=439, WT ACM=549, RTT ACM=633, RTT ACM + Igfbp2-Ab=621; FXS (**d**): alone=492, WT ACM=608, FXS ACM=621, FXS ACM + Igfbp2-Ab=647; DS (**f**):

alone=716, WT ACM=992, DS ACM=765, DS ACM + Igfbp2-Ab=858. Statistics by Kruskal-Wallis one-way ANOVA on ranks with Dunn's test for multiple comparisons. **g.** Application of an Igfbp2 neutralizing antibody reduces WT neuronal cell body size deficits induced by RTT ACM. Graph mean ± s.e.m., individual data points represent average per experiment, data from 3 experiments. Statistics by Kruskal-Wallis one-way ANOVA on ranks with Dunn's test for multiple comparisons. **h-l.** Delivery of an Igfbp2-neutralizing antibody increases cell body size of deep layer neurons in P7 visual cortex of RTT mice. **h.** Schematic: P2 mice were injected in the visual cortex with AAV synapsin-GFP +/− antibody, tissue collected at P7 and GFP-expressing neurons imaged. **i,j.** Cell body area in deep layer neurons is decreased in RTT compared to WT mice. **i.** Analysis by mice, graph average ± s.e.m., individual data points mice, N=4 WT, 4 RTT mice, statistics by 2-sided T-test. **j.** Analysis by cells, graph individual data points represent cells, dashed line at mean, n=133 WT, 189 RTT cells, statistics by 2-sided T-test. **k,l.** Cell body area in deep layer neurons in RTT mice is increased by an Igfbp2-Ab. **k.** Analysis by mice, graph average ± s.e.m., individual data points mice, N=5 control-Ab, 5 Igfbp2-Ab mice, statistics by 2-sided T-test. **l.** Analysis by cells, graph individual data points represent cells, dashed line at mean, n=219 control-Ab, 274 Igfbp2-Ab cells, statistics by 2-sided T-test. See also Extended Data Figure 5.

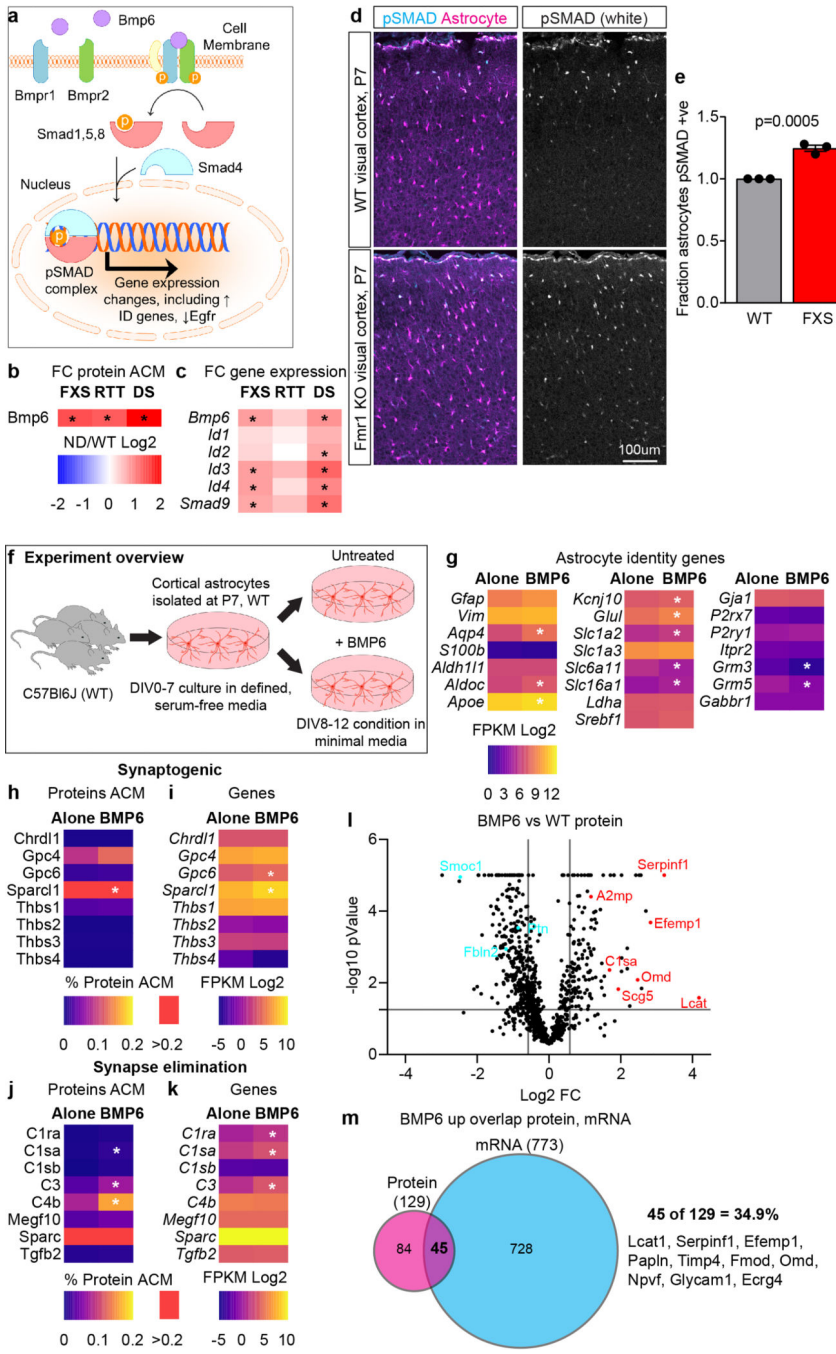

Figure 6. Activating WT astrocyte BMP signaling mimics ND astrocytes.

a. Schematic of canonical BMP signaling pathway. **b.** Fold change in BMP6 protein in ND ACM compared to WT. **c.** Fold change in gene expression for BMP family members in ND astrocytes compared to WT. Proteomics, N=6 cultures per genotype, *p<0.05, abundance >0.01%, fold change between WT and ND ≥1.5 calculated with T-fold test in Patternlab. RNASeq, N=6 cultures WT, RTT, FXS; 4 cultures DS, *adjusted p<0.05, FPKM>1, fold change between ND and WT ≥1.5 calculated with DESeq2. **d,e.** Increase in the proportion of pSMAD+ astrocytes in FXS visual cortex at P7. **d.** Example images

of astrocytes (magenta, Aldh1l1-GFP) and pSMAD (cyan) in the visual cortex at P7 of WT (Fmr1+/y) and KO (Fmr1-/y). **e.** Quantification of the proportion of astrocytes that are positive for pSMAD. N=3 WT, 3 FXS mice; bar graph mean±s.e.m., individual data points mice; statistics by 2-sided T-test. **f.** Experimental schematic for BMP6 treatment of WT astrocytes. **g-m.** Characterization of protein secretion and gene expression profiles of BMP6-treated WT astrocytes compared to untreated WT. **g.** Heatmap of astrocyte identity and function markers. **h-k.** Heatmaps of synaptogenic proteins (**h**) and genes (**i**), as well as synapse eliminating proteins (**j**) and genes (**k**). For the heatmaps a darker shade of red indicates a value above the top of the scale. **l.** Volcano plot of proteins present in ACM at >0.01%, plotted as Log2FC against -log10 p-value comparing BMP6-treated and untreated WT ACM. Each dot represents a protein; top right sector proteins significantly upregulated (FC>1.5, p-value <0.05), examples in red; top left sector proteins significantly downregulated (FC<−1.5, p-value <0.05), examples in turquoise. **m.** Venn diagram showing overlap between proteins and genes with increased expression in WT astrocytes following BMP6 treatment. For mass spectrometry and RNA Sequencing N=6 cultures, half of each culture treated with BMP6 and other half left untreated. Proteomics, *p<0.05, abundance >0.01%, fold change ≥1.5 calculated with T-fold test in Patternlab. RNASeq, *adjusted p<0.05, FPKM>1, fold change ≥1.5 calculated with DESeq2. See also Extended Data Figure 6; Tables S2,3,5,6,7,8,9.

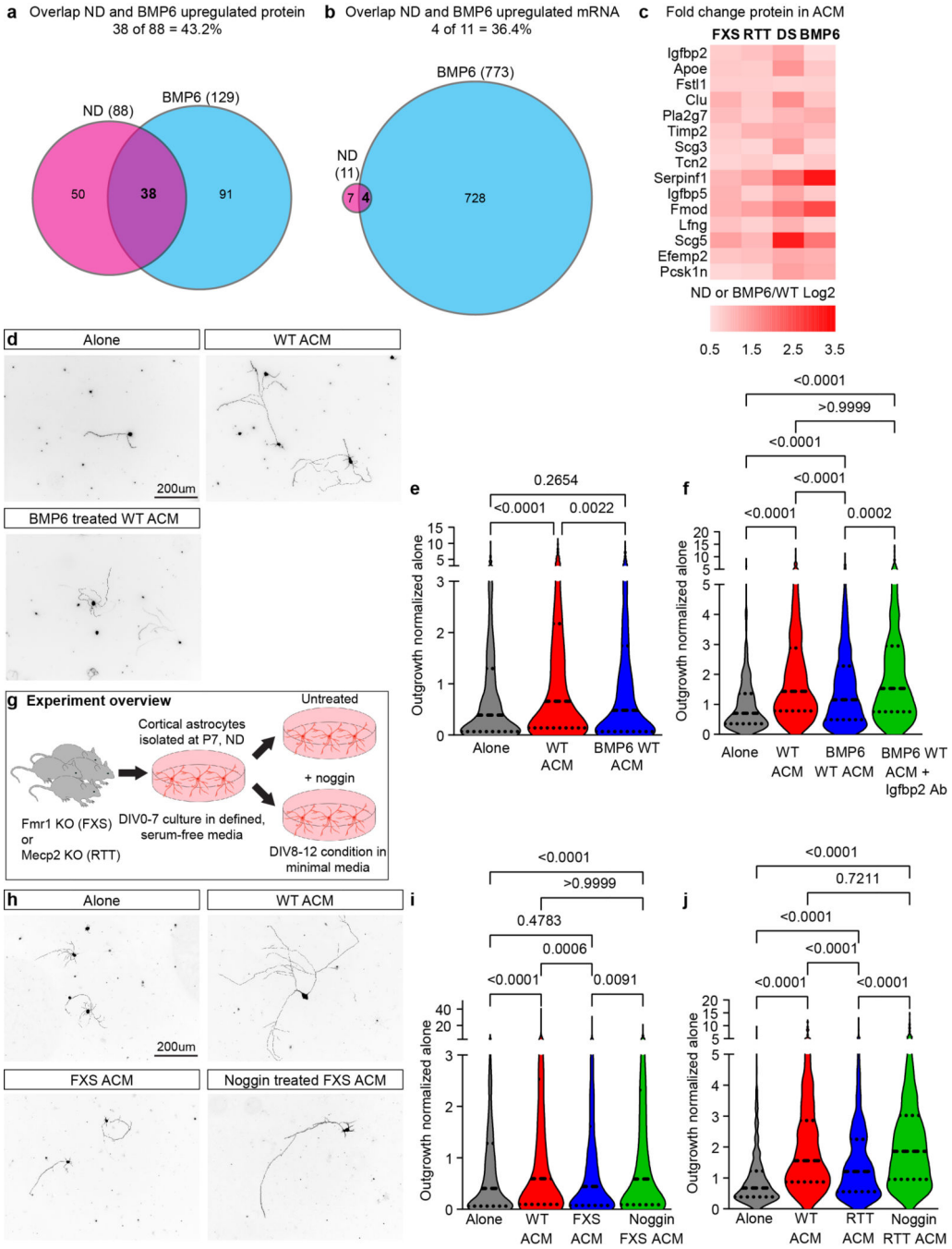

Figure 7. Blocking ND astrocyte BMP signaling reduces neural deficits.

a-c. BMP6-treated WT astrocytes show upregulated protein secretion (**a**) and gene expression (**b**) that overlaps with ND astrocytes. **c.** Heatmap of proteins increased in all ND and BMP6-treated astrocytes vs. WT, ranked by protein abundance in BMP6-treated ACM. N=6 cultures each WT, FXS, RTT, DS, plus 6 cultures WT +/− BMP6. **d,e.** ACM from WT astrocytes treated with BMP6 inhibits WT neurite outgrowth. **d.** Example images of WT neurons cultured for 48 hours, conditions as marked (merged images of MAP2 + Tau). **e.** Quantification of total neurite outgrowth. Data from 3 experiments, number of

neurons: alone=467, WT ACM=733, BMP6 WT ACM=610. **f.** Blocking Igfbp2 overcomes the inhibitory effect of BMP6 WT ACM on neurite outgrowth. Data from 3 experiments, number of neurons: alone=378, WT ACM=380, BMP6 WT ACM=506, BMP6 WT ACM + Igfbp2 blocking Ab=335. **g-j.** Blocking BMP signaling in ND astrocytes rescues deficits in WT neurite outgrowth. **g.** Experimental schematic for noggin treatment of FXS or RTT astrocytes. **h.** Blocking BMP signaling in FXS astrocytes rescues deficits in WT neurite outgrowth. Example images of WT neurons cultured for 48 hours, conditions as marked (merged images of MAP2 + Tau). **i.** Quantification of total neurite outgrowth. Data from 3 experiments, number of neurons: alone=923, WT ACM=1164, FXS ACM=1132, Noggin FXS ACM=1099. **j.** Blocking BMP signaling in RTT astrocytes rescues deficits in WT neurite outgrowth. Quantification of total neurite outgrowth. Data from 3 experiments, number of neurons: alone=238, WT ACM=279, RTT ACM=387, Noggin RTT ACM=365. Violin plot: dashed line median, dotted lines 25^{th} and 75^{th} percentile. Statistics by Kruskal-Wallis one-way ANOVA on ranks with Dunn's test for multiple comparisons. See also Extended Data Figure 7; Tables S5, S7.